

Chapter 6

Network Technologies for SDM



Werner Klaus, Jun Sakaguchi, Benjamin J. Puttnam, Nobuhiko Kikuchi,
Yong Lee, and Kenichi Tanaka

Abstract Traffic demands on the Internet are becoming increasingly dynamic and are driving the need for greater routing flexibility in the underlying optical network. Space-division multiplexing (SDM) is mainly seen as a means to increase data throughput and handle exponential traffic growth. But, its role is certainly more diverse. Research on SDM encourages device integration, brings new functionality to network elements and helps optical networks to evolve. As a result, the number of individual components in the future networks will decrease, which in turn will improve overall reliability as well as lower operational expenditure and power consumption. From an application point of view, the prevalence of various band-consuming applications such as video streaming, cloud computing, big data, Internet of Things (IoT), social networking service (SNS) will produce a strong traffic demand especially on short-reach fiber transmission links. Among them, inter- and intra-data center (DC) traffics are expected to grow very rapidly in the coming years, and the development of ultra-high-capacity data interconnection and network technologies is urgently needed. Such short-reach links are promising candidates of the first-stage introduction of SDM technologies not only because of the highest traffic demands but also due to relaxed fiber specifications that come hand in hand with the shorter transmission distance. The first part of this chapter introduces basic technologies devised for network nodes and reviews recent research which has extended the SDM concept to optical switching as well as has utilized SDM-specific features to facilitate network control. The second part then focuses on short-reach systems and discusses an application example of SDM for data center signal protection.

Werner Klaus is a chapter editor.

W. Klaus (✉) · J. Sakaguchi · B. J. Puttnam
National Institute of Information and Communications Technology, Koganei, Tokyo, Japan
e-mail: klaus@nict.go.jp

N. Kikuchi · Y. Lee · K. Tanaka
Research & Development Group, Hitachi Ltd., Kokubunji, Tokyo, Japan

6.1 Basic Technologies for Network Nodes and Network Control

Introduction

Space-division multiplexing (SDM) is considered the final frontier of multiplexing schemes to deal with the ever-increasing demand for transmission capacity in optical fiber networks. Many impressive experiments based on few-mode fiber (FMF) [1], multi-core fiber (MCF) [2] or few-mode multi-core fiber (FM-MCF) [3] have already clearly demonstrated the potential of SDM. Yet, just having large capacity is not enough for these SDM technologies to be commercially successful or to be accepted as a viable alternative to the already well-established transmission technology based on single-mode fibers (SMFs). As with any new technology, to make SDM attractive to network operators, it has to provide significant benefits in terms of cost and energy per bit. In addition, it must also offer a scenario that allows for a smooth transition from today's constantly growing SMF networks where fiber cables, once installed in the ground or under sea, are the most difficult and expensive part to replace [4]. From a commercial point of view, one may expect, therefore, that the SDM revolution will start on a small scale inside isolated network elements such as transponders, optical amplifiers and optical switches where the cost benefit of integration is the highest. As such, the development of SDM has to closely follow the evolution of today's optical networks and must be able to support photonic switching and routing with reconfigurable optical add/drop capability. In order to succeed, SDM will have to provide network elements with comparable performance but of lower cost than SMF-based devices when processing similar bitrates. Such a cost advantage can only arise if spatial multiplexing inside those elements can sufficiently leverage component sharing and integration.

To date, most research in the field of SDM is still concentrating on the improvement of transmission quality and the capacity-distance product. In contrast, this section will review work, not yet as extensive but still as important, which has been done in bringing SDM to the network nodes, as well as incorporate its concept to manage and optimize data flow in networks. The first part mainly focuses on the wavelength selective switch (WSS), a key enabler of transparent wavelength routing in today's optical networks. In the second part, we then discuss ideas and proposals on how to adapt network control and management to the SDM era as well as on how to utilize the spatial dimension for network optimization.

6.1.1 *SDM Switching and Node Elements*

6.1.1.1 Basic Components of a Network Node

Next-generation optical networks will most likely have a mesh topology with reconfigurable optical add-drop multiplexers (ROADMs) installed at its nodes. The

ROADM is a sophisticated *optical switch* that allows individual wavelength bands to be dropped from or added to the stream of wavelength-division-multiplexed (WDM) signals passing through the network node [5]. An example of a multi-degree ROADM architecture is shown in Fig. 6.1. The degree of a ROADM refers to how many fiber routes (or fiber pairs as most links are bidirectional) of the network are connected to the ROADM. A wavelength channel can be switched through (express path), removed from the WDM stream by forwarding it to a transponder (drop path) or inserted into the WDM stream from a transponder (add path). The switching performance of a ROADM is measured by functionalities such as colorless, directionless and contentionless (CDC). *Colorless* stands for the ability of the add/drop ports to access any wavelength of the incoming WDM stream, *directionless* stands for the ability to access wavelength channels coming in from any direction, and *contentionless* refers to the ability of not blocking wavelengths that are forwarded to the same drop port (but are processed by different transponders behind that port). The higher the functionality, the more complex and expensive the ROADM becomes. A CDC-ROADM is currently the most flexible but also the most expensive ROADM on the market.

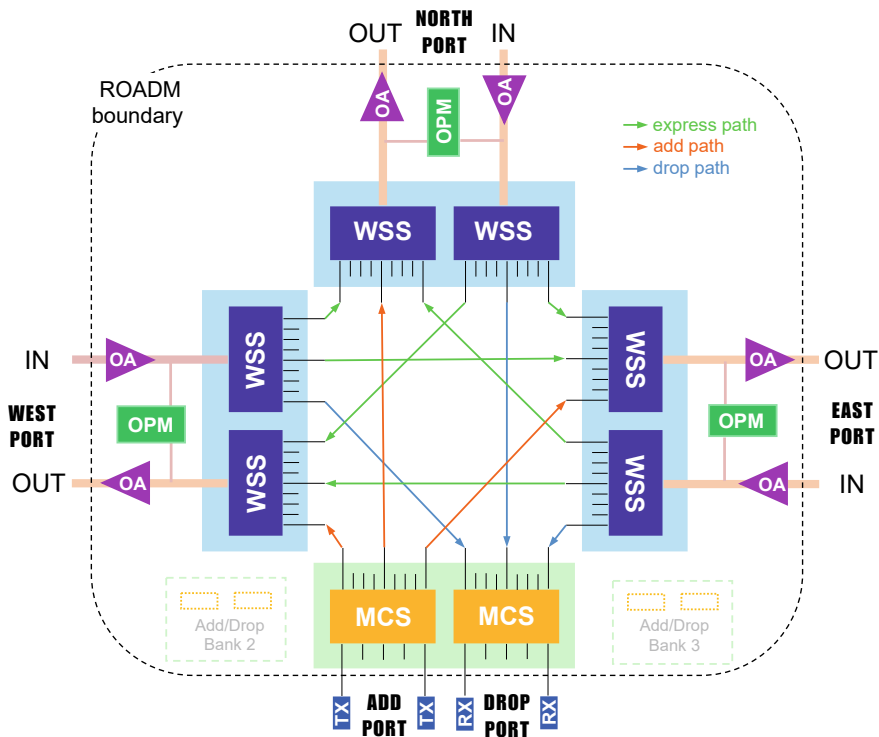


Fig. 6.1 Example of a degree-three CDC-ROADM (WSS: wavelength selective switch, OA: optical amplifier, OPM: optical performance monitor, MCS: multicast switch, TX/RX: transponders with coherent transmitters and receivers)

In addition, simulations of dynamic traffic in realistic networks have shown that in conjunction with a contention-aware routing and wavelength assignment scheme or algorithm, similar low blocking rates could be achieved also without the more expensive contentionless feature [5]. Nevertheless, the additional cost may be justified eventually with the provision of an extremely flexible hardware-based connectivity mechanism in the optical layer. Therefore, the CDC-ROADM is expected to serve best the needs of future networks which will require a high degree of network protection (against interruptions and component failures) as well as mesh restoration, optimization such as wavelength grooming or network defragmentation and most importantly quick adaptation to unpredictable traffic patterns including requests from large-bandwidth applications. On top of this, these functions need to be software controllable and provide performance monitoring from a remote location.

On the hardware side, the ROADM typically comprises several wavelength selective switches (WSSs) [6, 7], optical amplifiers, performance monitors, power splitters and spatial switches or a combination thereof, e.g., in form of a multicast switch (MCS). The WSS is the ROADM's key element. Its main job is to optically route wavelength channels between a single port on one side and N ports on the other side (commonly referred to as "1xN"). Since the WSS is optically bidirectional, the flow of wavelength channels can occur either from the single port to any of the N ports, or from any of the N ports to the single port (by means of selective channel blocking). Another job of the WSS is to attenuate each wavelength channel independently for the purpose of amplitude equalizing and power balancing in the network.

Figure 6.2 illustrates the operating principle of a 1×2 WSS. The light of the input fiber carrying an WDM signal is collimated and passes through polarization dispersive and beam shaping optics before it reflects off a diffractive grating that disperses (e.g., horizontally) the WDM signal into many beams with different propagation angles according to their wavelengths. Diffraction efficiency of the grating is increased by aligning the polarization to the grating grooves and illuminating as many grooves as possible with elliptically shaped beams. The beams are then converged by a lens (i.e., optically Fourier transformed) to a steering element which consists either of an array of micro-electro mechanical system (MEMS) mirrors or reflective liquid crystal on silicon (LCoS) pixels. By electronically controlling the tilt of a MEMS mirror or the amount of phase retardation in the LCoS pixels, the wavelength separated beams corresponding to different wavelength channels of the WDM signal are then deflected vertically toward different output ports. The wavelength (frequency) band of the light that is sent to a specific output port is determined by the total width of elements that steer the beam. This width is commonly set in accordance to ITU recommendations [8], e.g., frequency slot widths ranging from 50 GHz down to 12.5 GHz. A steering element may consist of a single micro-mirror in case of MEMS or many pixels in case of LCoS. The higher spatial resolution and flexibility in modulating a beam's amplitude and phase make the LCoS-based WSS currently the preferred choice for applications using a flexible wavelength grid.

The introduction of the WSS in the network nodes marked a major milestone in the network evolution from opaque networks, i.e., networks that perform the switching

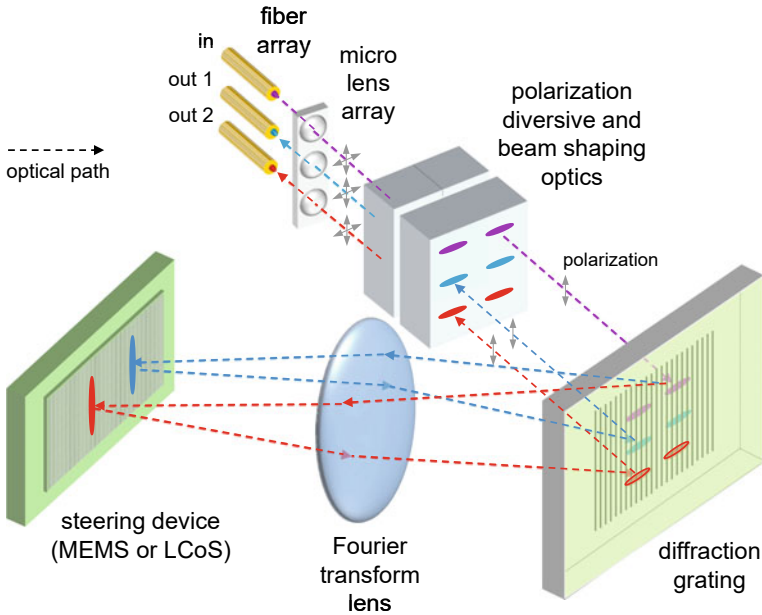


Fig. 6.2 Operation principle of a WSS (some optical paths have been omitted for clarity)

operations in the electrical domain by relying on power-consuming optical-electrical-optical (OEO) conversion to transparent networks, i.e., networks that switch and route WDM signals solely in the optical domain. With such a critical network element at hand, it is clear that incorporating spatial multiplexing into the WSS concept without increasing much the component count and footprint has to be also a primary concern of SDM research.

6.1.1.2 ROADMs and WSS for SDM Systems

The first SDM ROADM in conjunction with a simple MCF network was reported by Feuer et al. [9]. It comprised two 1×2 WSSs for seven-core MCFs that were made out of one commercial (SMF-based) 1×23 WSS by adjusting the output port assignment and MEMS mirror tilt angles. The operating principle of the resulting $7 \times (1 \times 2)$ WSS is shown in Fig. 6.3.

Spatial demultiplexers or fan-out elements were used to connect the cores of the MCF to the input ports of the WSS. Inside the WSS, all light beams associated with the same MCF are treated as a single entity and switched together by one steering mirror to one of the two output ports. The spatial extension of the grating (omitted in Fig. 6.3a) allows efficient separation of the wavelengths in parallel, but switching the beams as a group necessitated a larger steering angle, although it was also suggested that interleaving the input and output beams can reduce the steering angle [10].

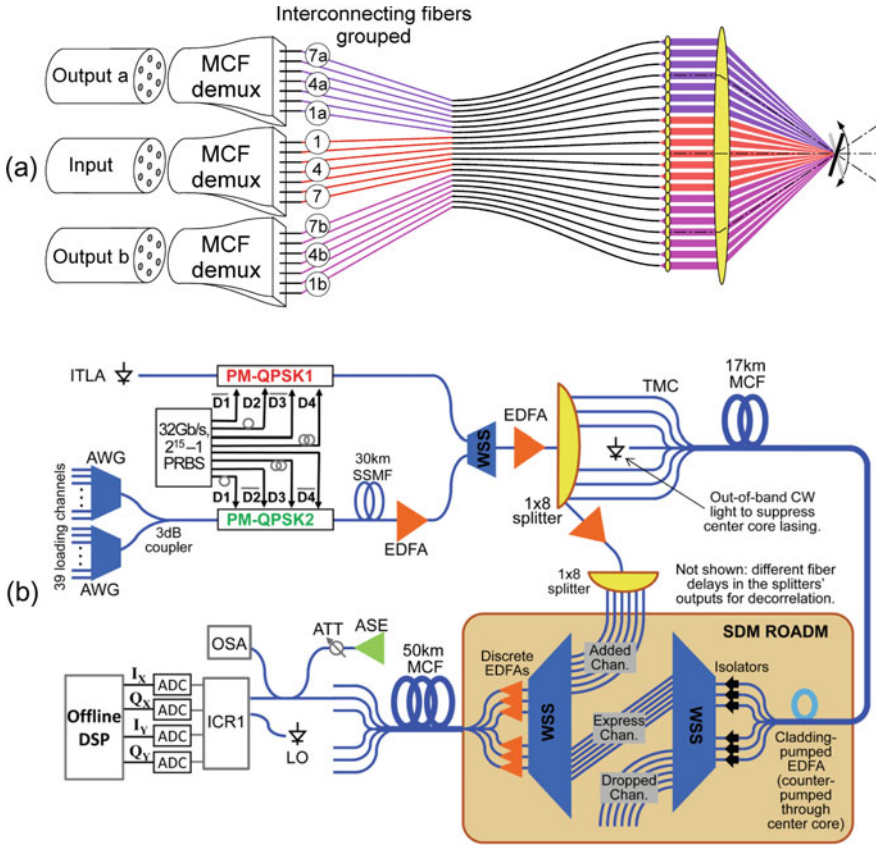


Fig. 6.3 a Operation principle of a $7 \times (1 \times 2)$ WSS. b Experimental setup for MCF transmission experiment with SDM ROADM (PM-QPSK: polarization-multiplexed quaternary phase-shift keying, PRBS: pseudorandom bit sequence, EDFA: erbium-doped fiber amplifier, TMC: tapered multi-core coupler, OSA: optical spectrum analyzer, ASE: amplified spontaneous emission, ATT: attenuator, ADC: analog-to-digital converter, DSP: digital signal processor) (Reprinted with permission from [9]. ©2013 Authors)

As shown in Fig. 6.3b, in the actual experimental setup, the two 1×2 WSSs were connected in a back-to-back fashion to provide the express, add and drop paths. Only the six outer cores of the incoming MCF were used as signal channels, while the MCF center core was reserved for pumping backward a cladding-pumped MCF erbium-doped fiber amplifier (EDFA) used as the ROADM’s input amplifier. Amplification at the ROADM’s output port was carried out by six discrete SMF EDFAs before inserting the light back into the next MCF span by means of a fan-in element. The loss of each WSS was kept below 5 dB at all test wavelengths. However, it was pointed out that the SDM WSS in this particular configuration is not able to correct (or balance) gain differences across the spectra of different cores that typically arise

due to non-uniformities in the MCF-EDFA's gain and fan-in/fan-out elements' loss characteristics.

Next, Ryf et al. [11] measured the performance of a WSS when using FMFs with three spatial modes at the input and output ports. The operating principle is similar to the SMF-based device with an LCoS steering device shown in Fig. 6.2, except that the collimator lens array at the input has to collect light from the FMFs. Similar to the previous approach, the spatial modes are treated as a single unit and switched together in the wavelength domain. Since the collimator lens array at the input was not designed for the FMF's smaller numerical aperture (NA), the spectrally separated beams did not properly focus in the LCoS plane causing excess loss and reduced spectral resolution. The measured insertion loss (IL) and mode dependent loss (MDL) ranged from 5.6 to 9 dB and 2.5 to 7.1 dB, respectively. Although the increased MDL restricted the transmission bandwidth, transmission above a Q-factor of 7.7 dB (equivalent to a BER of less than 7.6×10^{-3}) with 32 100 GHz-spaced 30-Gbaud QPSK WDM channels was achieved for up to six consecutive passes through a fiber loop incorporating the FMF-WSS and a 30 km FMF. However, even with FMF-optimized optics, each mode will still have a different spatial extension at the steering device precluding the possibility of obtaining the same spectral resolution for all modes. Different transmission bands and MDL are thus unavoidable and bring about the need for larger guard bands between the channels, as compared to SMF-based devices. The problem escalates with the number of modes the WSS has to deal with.

This problem can be solved by converting the higher-order modes to fundamental modes, e.g., with a photonic lantern (PL) [12, 13]. The PL has a similar job as the fan-in and fan-out elements discussed earlier with respect to MCFs, but instead of breaking out a number of closely spaced cores, it transforms a multi-mode input signal into several single-mode output signals. If the transition from the multi-mode to the single-mode section is lossless (adiabatic), as can be achieved by slowly varying the dimensions of a waveguide in the form of a taper along the propagation direction, then the mode conversion itself becomes also lossless, provided the number of single-mode signals at the output equals the number of the guided modes at the input. Such an approach was adopted by Carpenter et al. [14] who used a commercial twin 1×24 WSS to build a 1×11 FMF-WSS supporting three spatial modes. After mode conversion, two output ports of each PL were connected to one 1×24 input array of the WSS, whereas each PL's third output port was connected to the second 1×24 array. Figure 6.4 shows the MDL and IL characteristics for the spectral passbands ranging from 10 to 100 GHz. In this case, the transmission bands were not MDL limited anymore clearly demonstrating the benefits of manipulating light inside the WSS from only the fundamental mode.

This approach was further extended to six spatial modes by Fontaine et al. [15]. Instead of the typical 1D fiber array at the WSS input, a 2D array was introduced to process simultaneously a larger number of spatial channels. As shown in Fig. 6.5, the output ports of a six-mode PL were connected to six SMF input ports of the WSS arranged in a matrix fashion of two rows and three columns. All six beams associated with one input FMF are then directed via a 2D collimator lens array to the diffraction

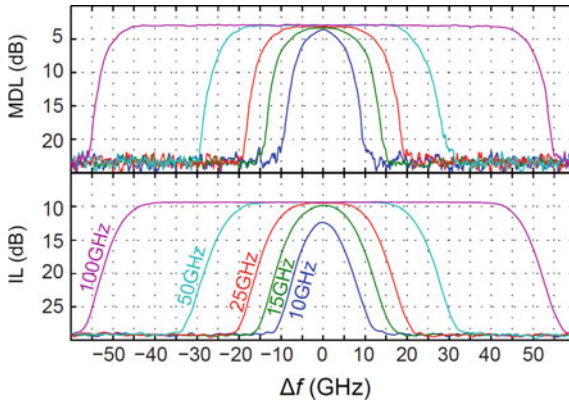


Fig. 6.4 Insertion loss (IL) and mode dependent loss (MDL) characteristics (Reprinted with permission from [14]. ©2014 The Optical Society)

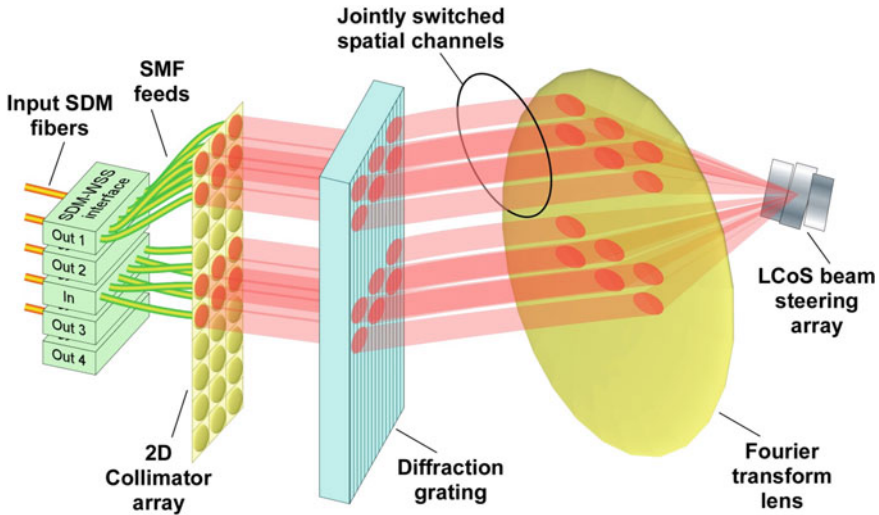


Fig. 6.5 FMF-WSS for six spatial modes (Reprinted with permission from [15].© 2015 Authors)

grating and focused onto the same LCoS steering element that deflects all six beams by the same amount. Since the number of modes to be switched simultaneously is twice the number of columns, the steering action has to skip every other row when deflecting the light to a 2×3 array of output ports. The WSS exhibited 5–8 dB insertion loss and a 0.5 dB spectral resolution of 78 GHz for 100-GHz-spaced channels.

When designing a WSS for SDM networks, the additional dimension of space can be utilized in two ways, to increase either the switch’s throughput or granularity. Most of the experimental demonstrations are thus far placed priority on increasing

throughput by means of “joint switching” of all available spatial channels simultaneously. For an SDM system based on FMF, such a choice is a natural consequence of the unavoidable mode coupling occurring along the fiber and the required MIMO DSP at the receiver. It would simply make no sense to route individual modes in the nodes when they need to be sent through the network as a unit anyway. On the other hand, if the SDM system is based on low-crosstalk MCFs, no constraints are imposed from the side of the transmission medium, and as we will see in the following section, there may be instances in a network where an increased granularity or the availability of an additional switching dimension can be more beneficial than an increased throughput.

Finally, we note that the generalization of the $1 \times N$ WSS would be a $N \times M$ wavelength selective optical cross-connect (WS-OXC). The WS-OXC is the ultimate flexible switch in a network node that can route any wavelength from any of N input ports to any of M output ports. Such OXCs are very complex (e.g., when realized with cascaded WSSs) and have found thus far only limited application in SMF networks due to cost restrictions. However, as we have seen from the previously discussed examples, the tight transmission band and insertion loss tolerances of WSSs will most likely restrict optical processing inside the WSS to beams with minimum spatial extension, i.e., the fundamental waveguide mode or Gaussian beam. The design principles of OXCs developed today for SMF networks may thus equally be applied to SDM networks in the future. In this respect, a clever design for an all-optical WS-OXC was recently proposed by Fontaine et al. [16]. This optical switch featured a full cross-connect with flexible passbands and had a similar amount of component building blocks and footprint as a single $1 \times N$ WSS. The optical layout and working principle is shown in Fig. 6.6. Although this device was not specifically developed with SDM in mind, it represents a good example of how the need for parallelization and integration stimulates advanced designs that utilize “space” and some yet unexploited parallel processing capabilities of optics more efficiently in network elements.

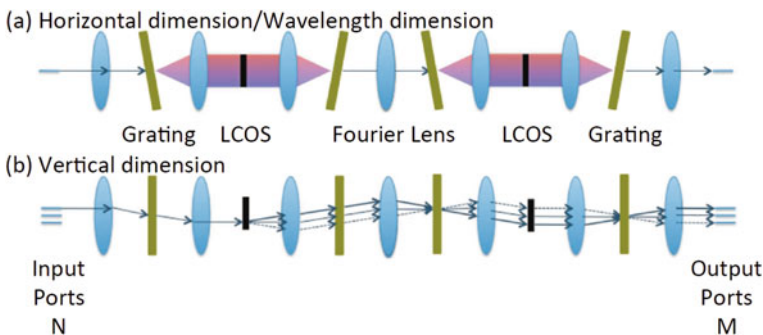


Fig. 6.6 Operation principle of wavelength selective OXC (Reprinted with permission from [16]. ©2013 IEICE)

6.1.2 SDM Network Control and Node Configuration

6.1.2.1 Architecture of Optical Networks

The technological achievements in the field of optical communications over the past few decades have enabled and supported a dramatic growth in traffic on the Internet. As the human mind is intrigued by the idea of accessing any kind of information from anywhere at any time with the highest possible quality, this trend is likely to continue for the coming decades. Mobile broadband and multimedia applications as well as machine-to-machine communication and cloud computing are fueling the need of using the network's optical and electronic resources as efficiently as possible in terms of capacity, cost per bit and power consumption.

One way to increase efficiency in a network is to make it flexible and elastic, i.e., provide some means that let the network dynamically adapt to unpredictable traffic patterns and rapidly establish or tear down connections through software. The goal of the flexible network is to utilize the available bandwidth more efficiently by introducing a frequency grid for the optical carrier frequencies (wavelengths) with a granularity four times finer than the 50 GHz spacing used in traditional networks. An architecture based on such a flexible grid will allow the network operator to match better heterogeneous traffic requests with different bandwidths. The LCoS technology of WSSs is well-suited to deal with such requirements. Note that, in the context of elastic networks, the WSS designed for flexible grids is sometimes referred to as spectrum selective switch (SSS). Elasticity is introduced into a network by employing configurable optical hardware, e.g., the ROADM, and by making the provisioning process of the end-to-end connections software controllable. As data center access and cloud computing increasingly dominate the traffic on the Internet, dynamic configurability and controllability are considered indispensable for provisioning the required quality and performance of future data links.

The network architecture is mainly determined by the hardware installed in a network node and the software controlling it. On the hardware side, various types of advanced optical network elements have been developed over the years of which the ROADM is a prominent example. The introduction of the ROADM has significantly reduced the amount of expensive and power-consuming electronic equipment in the node. It has changed also the notion of a network node of being a point of regeneration to being a point of routing. *Routing* stands for the process of selecting a path through the network based on a certain traffic demand. Another important aspect of network management is *wavelength/spectrum assignment*. The term *spectrum assignment* is commonly used in the context of elastic/flexible optical networks. In combination with the task of routing, these processes are referred to as the routing and wavelength assignment (RWA) problem or the routing and spectrum assignment (RSA) problem. A number of algorithms have been developed to solve these problems, and cost-effective and efficient network design today relies heavily on such algorithms. Another major contribution from the software side toward dynamic networking has been the introduction of software-defined networking (SDN) [17]. SDN acts as a

network-wide operating system that allows unified and dynamic control of the data flow through the network devices in a flexible manner. Most importantly, routing tasks and traffic engineering can be performed with software developed independently from the node hardware.

Although the functionalities of ROADMs are being constantly improved, their architecture based on hard-wired device connections may eventually limit them in terms of scalability to deal efficiently with heterogeneous traffic requests in a dynamic network. A possible solution for scalable optical switches is offered by a multi-granular architecture [18]. Increased flexibility and scalability are realized by splitting up the switching process into several layers of switching granularities such as on a per-fiber basis, a per-waveband basis or a per-wavelength basis. A waveband represents here a set of contiguous wavelength channels that is treated as a single unit with respect to add/drop or node bypass. The layers can be implemented either with separate OXCs or collapsed into a single switching fabric. The latter has led to the important concept of Architecture-on-Demand (AoD) [19]. As shown in Fig. 6.7, an AoD node consists of an optical backplane, e.g., implemented by a large port-count 3D-MEMS switch, to which several pluggable modules are connected providing a set of signal processing functions, such as optical amplification, spectrum/wavelength/subwavelength switching, wavelength conversion, and signal regeneration. Subwavelength switching refers here to the process of subdividing a single wavelength channel further into timeslots by means of a fast time-multiplex scheme.

Based on traffic requirements, an AoD synthesis algorithm calculates a synthetic node design that provides the required functionality. AoD is flexible and modular, facilitates provisioning, simplifies the introduction of new functionalities and supports arbitrary granularities. On the other hand, the development of an AoD algorithm that can calculate the optimal node architecture while taking into account cost and availability of architecture-building modules as well as traffic dynamics may be very complex. Furthermore, the benefit of increased flexibility needs also to be balanced with a larger footprint and power consumption of the node due to the additional MEMS switch [20].

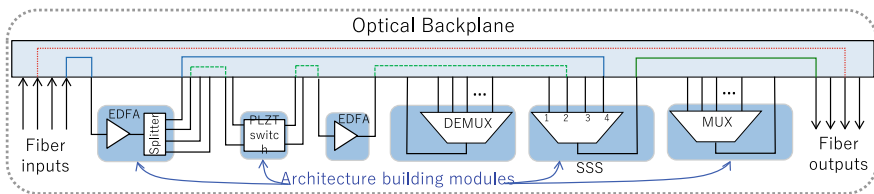


Fig. 6.7 Example of an AoD node configuration

6.1.2.2 Control and Management of SDM Networks

The introduction of SDM into the network will increase capacity and switching flexibility, but it also adds new challenges to an already complex network control. Amaya et al. [21, 22] demonstrated in two experiments how the AoD architecture could be beneficial for SDM networks. In the first experiment, shown in Fig. 6.8, a network was set up comprising four programmable AoD nodes connected via two seven-core MCFs and several SMFs [21]. The optical backplane consisted of a 160×160 3D-MEMS optical switch interconnecting the fibers with several wavelength selective switches, optical amplifiers, power splitters and a fast lead lanthanum zirconate titanate (PLZT) switch for subwavelength switching. Switching across the space, frequency and time dimensions with a granularity range of over 6000 was demonstrated in Node 2. The maximum amount of traffic was achieved with core-to-core switching, where 939 Gb/s were switched with a single cross-connection. The minimum amount of traffic allocated was one timeslot in a 64-timeslot frame of a 10G subwavelength channel with 156 Mb/s.

The second experiment demonstrated the use of SDN to control a SDM network consisting of three AoD nodes, linked by several SMFs and two MCFs with 19 and 7 cores, respectively [22]. SDN provides four key features that make it suitable for such heterogeneous networks: Firstly, the data and control plane are separated which allows an independent evolution of the network and control software as well as network virtualization where the SDM infrastructure can be partitioned (sliced) into multiple logically isolated units. Secondly, the network control is centralized which leads to a better overview and stability of the network. Thirdly, open (i.e., vendor independent) interfaces are used between the software/hardware in the control and data planes which achieve plug-and-play operation of the network. And fourthly, programmability of the network by external applications due to the abstraction of the

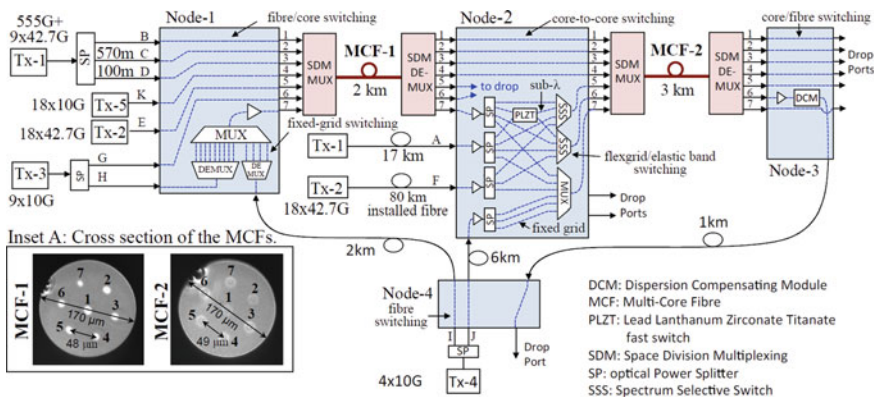


Fig. 6.8 Experimental setup of the multi-granular SDM network (Reprinted with permission from [21]. ©2013 The Optical Society)

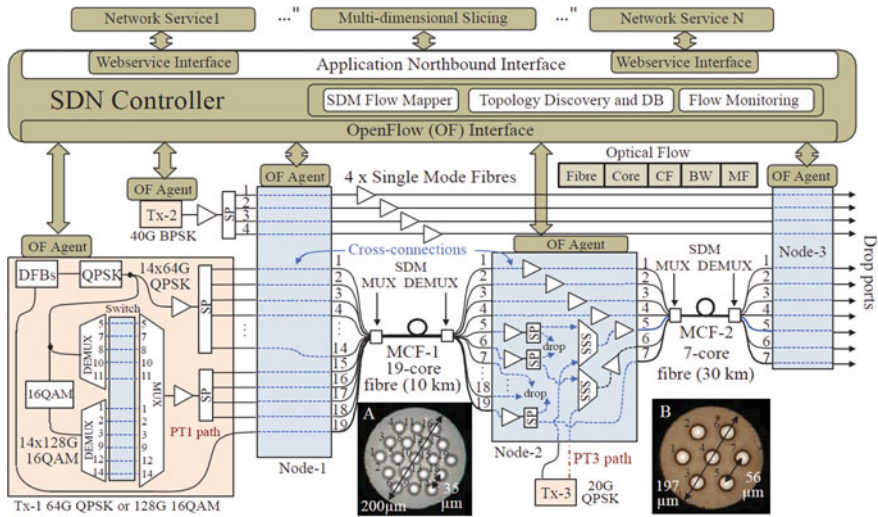


Fig. 6.9 Experimental setup of the SDN-controlled SDM network (Reprinted with permission from [22]. ©2014 The Optical Society)

underlying network infrastructure by the SDN controller enables fast development of new services and a rapid evolution of the network.

As shown in Fig. 6.9, the control plane includes an SDN controller and a multi-dimensional network slicing service (i.e., external applications). Communication between the control and data plane is carried out with an OpenFlow interface at the control plane side and OpenFlow agents at the data plane side. OpenFlow [23] is a standard protocol that acts as the control data plane interface to enable manipulation and centralized control of network devices by the SDN controller.

MCFs are abstracted as a single entity with multiple spatial channels whose information is used by the slicing service for routing spatial superchannels. A spatial superchannel is generated by grouping together signals on a number of spatial channels (i.e., cores) that operate at the same wavelength and thus provision more instantaneous bandwidth to a single request. For example, a 19-core MCF could be abstracted as a superchannel with 1.9 Tb/s per wavelength, while only 100 Gb/s (per wavelength) are carried by each core. On the other hand, SMFs are abstracted as multiple entities each with a single independent spatial channel and, therefore, are not suitable for transmitting spatial superchannels. An example of data flow using these different types of spatial channels is illustrated in Fig. 6.10. The SDN controller translates connectivity requirements such as source, destination and quality of transport (QoT) into physical layer requirements such as number of cores, wavelength, data rate and the modulation format. Each data signal is then assigned to either a single SMF core or a group of MCF cores representing a superchannel slice. In this way, flexible bandwidth provisioning from 40 to 512 Gbps in conjunction with different QoT requirements could be demonstrated.

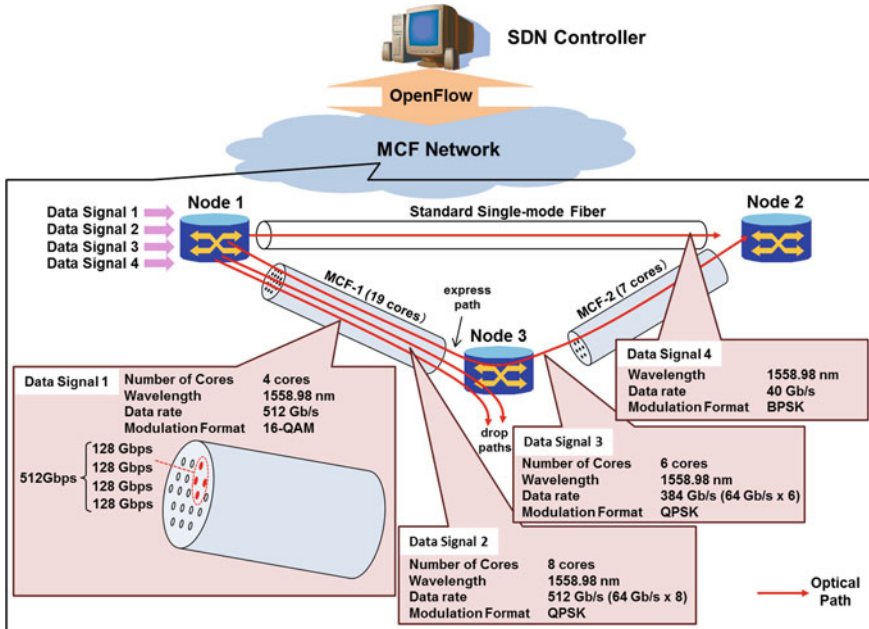


Fig. 6.10 Example of the heterogeneous data flow in an SDN-controlled SDM network with sliced spatial superchannels

The elastic node architecture in combination with a flexible resource allocation gives the network designer more freedom to optimize the traffic routed through the SDM network. Fujii et al. [24], for example, demonstrated how a smart spectrum and core allocation method could reduce spectrum fragmentation, blocking probability and node cost in a seven-core MCF network taking into account realistic topologies. Furthermore, they also showed that by including inter-core crosstalk between adjacent cores and information on the core position in the RSA problem, the impact of crosstalk from the perspective of the network can be significantly mitigated even under high traffic load [25].

6.1.3 Network Enhancements Due to MCF

Although the integration of parallel transmission channels almost always entails a certain amount of channel crosstalk, the physics of inter-core crosstalk in MCFs has been well-studied, and an adequate fiber design is likely to be able to mitigate it to negligible levels (see also Sect. 2.2). In the following, we summarize three features that are unique to low-crosstalk MCF transmission and thus may help enhance the performance of future networks.

(1) *Wavelength/spectrum contention management in the optical domain*

In an SMF network, different traffic demands with the same wavelength cannot be routed through the same link due to wavelength contention. To solve this problem without having to resort to OEO conversion, much hope has been placed in research on all-optical wavelength converters based on semiconductor or periodically poled lithium niobate devices as well as highly nonlinear fibers. However, the trend toward using digital coherent transmission techniques in the future optical networks may substantially limit the range of potential solutions. This in turn will make it also increasingly challenging to convert those research outcomes into efficient and practical products due to the intrinsic properties of the optical processes involved [26]. Therefore, it is likely that SMF networks will continue to rely on RWA/RSA algorithms and OEO regeneration to minimize the probability of blocking due to wavelength contention.

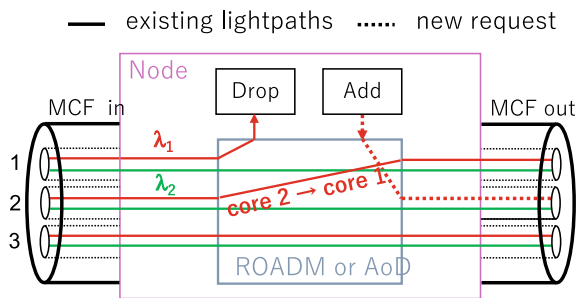
In an SDM network based on FMF, traffic requests with the same wavelength (but assigned to a different spatial mode) can be routed through the same link, but the add and drop points of the requests need to be the same due to mode mixing. Therefore, from the viewpoint of wavelength contention management, FMF networks offer no advantage over SMF networks.

In an MCF network, on the other hand, the wavelength contention problem could be further mitigated solely in the optical domain since core (spatial channel) switching can be easily incorporated in the node. A simplified example is shown in Fig. 6.11. When there is an add request with high QoT requirement against less-impaired but already-occupied channel (Core 2), the express traffic with less stringent QoT requirements can be temporarily switched to another (by the same wavelength) unoccupied spatial channel (Core 1) with less favorable transmission characteristics. The risk of having to block a new request can be effectively averted in the optical domain.

(2) *Sliceable spatial superchannels*

A spatial superchannel does not need to occupy all cores of an MCF, but it could also be formed out of one or more subsets of core groups referred to as superchannel slices thereby increasing switching granularity. The size (bandwidth) of these slices can be flexibly adjusted according to traffic demands as was already exemplified in Fig. 6.11. Note that, the concept of the spatial superchannel is based on the fact that

Fig. 6.11 Example of wavelength contention management with MCF



the phase shifts of signals due to environmental changes in MCF cores surrounded by the same cladding are much stronger correlated than in parallel strands of SMFs [27]. These correlations could be utilized to save in DSP complexity by sharing that phase information between DSPs in a master–slave configuration to jointly process the signals on the subchannels of a superchannel [28]

(3) *Bidirectional transmission in a single fiber*

Although it is possible to carry bidirectional traffic on a single SMF, it is not common practice to do so in today’s networks. Telecom carriers typically light up an additional pair of fibers when they need to add capacity to a link. On the other hand, MCFs are well-suited to handle bidirectional transmission in a single strand of fiber with the side benefit of significantly reducing the effect of inter-core crosstalk when assigning each direction to a core in an interleaved fashion [29, 30].

Conclusions

As network traffic continues to grow, the required physical layer capacity will most likely be provisioned in the near term by deploying more SMFs per link and deriving more flexibility from the underlying network technology. However, as network evolution strongly depends on a reduction of the cost per bit and to an increasing extent the energy per bit, it is also clear that this trend cannot go on forever and it may not take too long before a tipping point is reached where SMF networks with multiple fibers and separate network elements are no longer economically viable. The development of SDM technology and the associated trend toward greater device integration are a consequence of the continuing quest for more efficient optical networks. Besides new fiber types and amplification techniques, advances in node design and network management strategies are crucial to make efficient use of the last unexploited physical dimension in optical communications.

6.2 Application of SDM Technologies in Short-reach Systems

Introduction

The demand for large-capacity data transmission is rapidly growing driven by the expansion of broadband application services [31] in large-capacity short-reach transmission systems due to the ongoing increase in data traffic. Especially, network reliability has become a serious issue [32, 33] in large-capacity transmission systems. Some researchers have recently made avid appeals for the need to prepare for disabilities in communication networks [34, 35]. Space-division multiplexing (SDM) schemes utilizing multi-core fibers (MCFs) [36], on the other hand, have attracted a great deal of attention as promising technologies for overcoming the limitations in not only transmission capacity imposed by conventional single-core single-mode

fibers (SMFs) [37] but also cable size at data center (DC) networks and passive optical networks such as fiber to the home (FTTH) [38] in access areas, which have necessitated the use of high fiber counts and high-density cables. MCFs can provide protection lines for redundancy as well as primary high-capacity signal lines in addition to these capabilities and can thus create networks that are extremely reliable.

One such approach can be the network system with optical protection switches and MCFs for high capacity and high reliability: We recently propose its basic concept [39, 40] and have fabricated prototype protection optical switch units (POSUs) with MCFs, as well as compact fan-in/-out (FI/FO) modules and optical connectors for the MCFs. Automatic impairment-aware optical-path switching was experimentally demonstrated by configuring an MCF network with these units and components [41]. In this prototype, we focus on access networks for business [42] residential areas [43] in this study as targets that required reliability on the basis of business continuity plans (BCPs) [44, 45], since access networks have explosively expanded due to carriers and have been alternatively developed and improved. For instance, a DC in a business area has one base node as a rule of aggregation and several accompanying branch nodes [46, 47]. A core switch (SW) is prepared at the base node as an input/output (I/O) interface for access to an external system. The end-of-rack SWs/top-of-rack SWs are prepared at the branch nodes to access servers and storage. The network topology in such a DC is useful for operation under no centralized traffic by means of increasing numbers of aggregation nodes that prevent collisions between data and shorten the access time to servers [48, 49]. Moreover, such networks need to have highly reliable characteristics to prepare for unpredictable problems such as failures or sudden excessive usage.

After an introduction of some types of short-reach systems in Sect. 6.2.1, we discuss in Sect. 6.2.2 a novel MCF link based on a multi-ring structure to achieve robust access networks such as those in DC systems in business areas and FTTH systems in residential areas. We also present a switching control architecture that could suitably manage this network and was effective in recovering from failures that occurred in the network. An MCF connector and an MCF FI/FO module were developed to enable low-loss connection between units. We also experimentally investigated the fundamental operation of automatic impairment-aware optical-path switching when failures occurred in the proposed link.

6.2.1 *Types of Short-reach Systems*

6.2.1.1 High-capacity Data Interconnection

As the speed of short-reach optical links is getting higher and higher, the use of parallel transmission becomes more and more popular: Table 6.1 shows the examples of high-speed Ethernet standards over a last decade: To achieve higher total capacity, most of standards utilize the plural lanes using parallel optical fibers or a single

Table 6.1 Examples of high-speed Ethernet standards

Standard	Baud rate/format	Type	Reach	Number of lanes ^a
40GBASE-SR4	10.3125 Gbaud/NRZ	4MMF	100/150 m	4
40GBASE-LR4	10.3125 Gbaud/NRZ	SMF/4WDM	10 km	4
100GBASE-SR10	10.3125 Gbaud/NRZ	10MMF	100 m	10
100GBASE-SR4	25.78125 Gbaud/NRZ	4MMF	100 m	4
100GBASE-LR4	25.78125 Gbaud/NRZ	SMF/4WDM	10 km	4
100GBASE-DR ^b	53.125 Gbaud/PAM4	SMF	500 m	1
400GBASE-SR16	26.5625 Gbaud/NRZ	16MMF	100 m	16
400GBASE-DR4	53.125 Gbaud/PAM4	4SMF	500 m	4
400GBASE-FR8/LR8	26.5625 Gbaud/PAM4	SMF/8WDM	2 km/10 km	8

^aFor unidirectional connection

^bStandardization not completed

optical fiber with wavelength-division multiplexing (WDM) technique. Since the increase of number of lanes (transceivers) leads to significant increase of cost, power and transceiver size, it is kept to less than four in many standard categories.

With the 10-times capacity increase from 40 to 400 GbE, the maximum channel rate is also increased by 10 times from binary 10 Gbit/s (10 Gbaud NRZ) to 100 Gbit/s (50 Gbaud PAM4) with the use of high-speed multilevel modulation [50, 51], which keeps the number of lanes to four. But, the use of 50 Gbaud PAM4 signal is currently limited to less than 500-m SMF categories (100GBASE-DR and 400GBASE-DR4 in Table 6.1), mainly due to the reduction of power budget of high-speed PAM signals. In the case of 400GBASEFR8/LR8 with longer reach using WDM, the number lanes (wavelength) must be increased to eight. Further increase of channel speed to 100 GBaud or beyond is investigated; however, it will face issues of device bandwidth limitation and less transmission reach. For the case of less-expensive shorter-reach interconnection over multi-mode fiber (MMF) commonly used in intra-building or rack-to-rack cabling, the number of signal lanes required for bidirectional connection is increased from 8 to 32 in the case of 400GBASE-SR16 [52].

In the future higher-speed interconnection like 1 Tbit/s or beyond, the number of signal lanes will increase more and more, due to the limits of both physical lane speed and number of wavelength: For example, to realize a 1.6-Tbit/s interconnection, the number of signal lanes (unidirectional) is expected to increase up to 64 for 10-Gbaud binary signaling, 32 for 25-Gbaud PAM4 signaling, 16 and 8 for even 50-Gbaud and 100-Gbaud PAM4 signaling.

Today's parallel interconnection typically uses ribbon fibers with MTP™/MPO-type parallel connectors, which causes significant wiring problems even in today's DCs, network nodes or supercomputers: Jacketed ribbon fiber cables are thick, heavy, costly and difficult to handle. Their connectors are also expensive, bulky and consume precious front or back panel area. Also in large DC networks, the use of parallel multi-mode ribbon fibers causes differential modal skew problem which makes timing

adjustment of high-speed signals difficult [53]. Further increase of number of fibers in a single ribbon fiber or connector seems very difficult to achieve.

Future introduction of newly developed MCF-based data interconnection (possibly with even MCF-based ribbon fiber) is expected to relax these wiring problems considerably, reducing the number of fiber cables by one order of magnitude and will give future DCs precious margin for further expansion. At the same time, multi-mode MCF is expected to have much less differential modal skew compared with ribbon MMFs.

Table 6.2 shows recently proposed MCF links for short-reach data interconnections. Requirement on MCF for short-reach interconnections is considerably different from those of core networks: One major requirement is the choice of signal wavelength, and typically 0.85 or 1.3 μm is used in very short reach (up to 100 ~ 300 m) and short reach (up to 40 km) applications. For the very short-reach applications, MCF with multi-mode fiber core [54–56] is preferable to relax the coupling accuracy between optical devices and the fiber core and to reduce assembly cost. Single-mode MCFs are also required for short-reach applications, since transmission reach of high-speed signals over multi-mode core is seriously limited by its modal skew. Clad diameters of MCF should be 125 μm or similar, in terms of fiber handling, bending loss, fiber cable density and backward compatibility. On the other hand, core-to-core crosstalk specifications required for short-reach interconnection can be relaxed drastically since the amount of total crosstalk is proportional to fiber length.

Other considerations are the number of cores and the core arrangement: In terms of efficient use of cores, the core number for short-reach parallel interconnections should be compatible with the number of their signal lanes (e.g., Table 6.1). The core arrangement may be more important in terms of the coupling to optical devices; since fan-in/fan-out devices between MCF and single-core fibers are costly and bulky for low-cost short-reach interconnections, direct coupling between MCF to integrated lasers and photodetectors seems to be very favorable in the future. In some cases, square core arrangement [58, 59] may be favorable, since it is compatible to the arrangement of integrated optical devices.

Table 6.2 Proposed MCF links for short-reach data interconnection

Refs.	No. of core	Core arrangement	Core diameter or MFD/mode	Clad diameter (μm)	Wavelength
[57]	2	Dual (2)	10 μm /single	125	1.3/1.5 μm
[58]	4	Square (2×2)	10 μm /multi-	125	850 nm
[54, 55]	7	Hexagonal (6 + 1)	26 μm /multi-(GI)	125	850 nm
[59]	8	Square (2×4)	4.9 μm /single	200 ^a	1.5 μm
[60]	8	Circular (8)	8.4 μm /single	125	1.3 μm

^a Estimated from photograph

6.2.1.2 PON and Data Center Networks

Various studies were reported on new applications of MCF/few-mode fiber (FMF)-based SDM technologies for short-reach systems. One of such application areas is access network (e.g., [61, 62]). Zhu et al. [38] proposed the first application of MCF to increase the capacity of PON and successfully demonstrate parallel transmission of seven PON signals over 11.3-km seven-core MCF with 2.5-Gbit/s upward/downward signals and 1:64 splitting.

Further capacity increase was demonstrated by Li et al. [63], with an aggregating downstream capacity of 300 Gbit/s using six MCF cores with 10-channel WDM. Hu et al. [64] demonstrated mode-division multiplexing (MDM) PON with double capacity over using LP00 and LP01 modes of low modal coupling FMF and passive mode multiplexers/demultiplexers.

Another application of SDM technique in PON is the low-loss combining of multiple upstream signals: Instead of using a conventional power combiner, Nakanishi et al. [65] and Cheng [66] give the basic idea of using a mode combiner and a multi-mode (mode coupling) receiver for the lossless combining of PON upstream signals. Fujiwara et al. [67] propose a PLC-based hybrid upstream SM-to-MMF mode combiner/downstream conventional splitter (Fig. 6.12). The 1×16 prototype splitter shows 7.7-dB loss reduction from the ideal combining loss (12 dB), although the MMF length is limited to short distances.

Xia [68] further proposes the use of several-km long FMF and a mode combiner replacing conventional single-mode feeder fiber and a power combiner and demonstrated 20-km 3-mode transmission of commercial G-PON signal. Effenberger [62] further introduces the concept of PON upstream upgrade of lossless coupling configuration to mode group multiplexing by adding a mode splitter at the OLT side.

One of the issue of MMF feeder technique is a limited number of independent spatial mode unlike the case of long-distance transmission where MIMO technique is typically used to separate multiple spatial mode, since the use of computational-heavy MIMO calculation is not suitable to access networks. One approach to solve

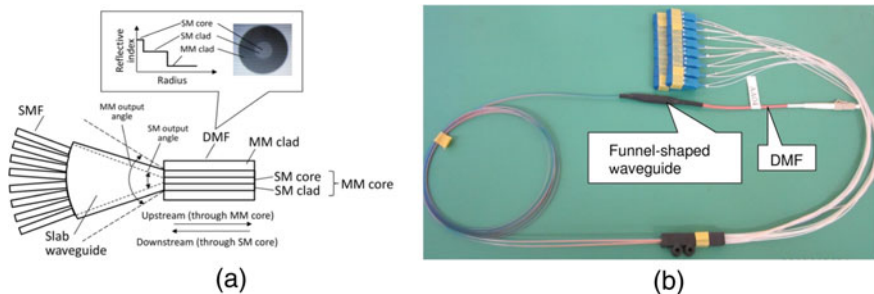


Fig. 6.12 Proposed optical splitter. **a** Configuration. **b** Photograph of 1×16 prototype (Reprinted with permission from [67]. ©2014 Authors)

this problem is the use of OAM multiplexing, and Fang [69] proposes its use with free-space optics (FSO) or vortex fiber and successfully demonstrated 20-mode multiplexing of 10-Gbit/s on-off keying (OOK) signals using a 0.4 m FSO setup. On the other hand, Effenberger [62] proposes that the computational load of the MIMO DSP of the FMF mode demultiplexing can be relaxed in the PON application due to a small differential modal group delay and the burst TDM signaling, which tend to enhance modal orthogonality.

The use of optical interconnection and optical SDM switches in the future data center is proposed and discussed in many papers (e.g., [53, 70–72]), and the introduction of MCF/FMF-based SDM technologies is expected in the future. Yan [73] proposes the intra- and inter-data center networking architecture utilizing WDM/TDM/SDM technologies and experimentally demonstrates their feasibility with the prototype utilizing three-element multi-element fiber (MEF) to handle top-of-rack SDM links and SDM-to-WDM conversion techniques based on fiber four-wave mixing (FWM) [74].

6.2.2 Application Example of SDM Technology in Short-reach Systems

A failure recovery system utilizing a multi-core fiber (MCF) link with protection optical switch units was developed to achieve high-capacity and high-reliability optical networks in short-range links. We describe the novel MCF link based on a multi-ring structure and a protection scheme to prevent link failures. Fan-in/fan-out modules and connectors were also developed in order to demonstrate the development status of the MCF connection technology for the link. We demonstrated path recovery by switching operation within a sufficiently short time (< 50 ms), which is required by ITU-T. The selection of a protecting path as a failed working path was also optimized as the minimum passage of units for low-loss transmission. The results we obtained indicate that our proposed link has potential for the network design of highly reliable network topologies in access areas such as data centers, systems in business areas and fiber to the home systems in residential areas.

The remaining part of this chapter is organized as follows: Sect. 6.2.2.1 explains the basic concept of the proposed MCF link, and Sect. 6.2.2.2 describes the POSUs, MCF FI/FO modules and MCF connectors used for the MCF link. Section 6.2.2.3 then discusses the MCF link based on a multiple ring structure, the switching control architecture, failure recovery scheme and switching control architecture. Section 6.2.2.4 details an experimental demonstration for recovery from link failures in the ring structure. Finally, in conclusion, we summarize our findings.

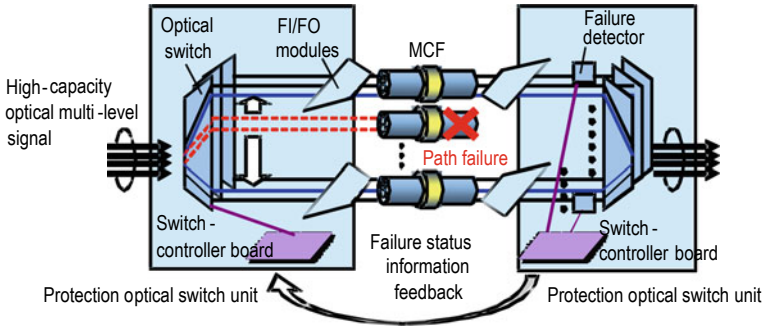


Fig. 6.13 Configuration of the proposed MCF system

6.2.2.1 Concept of Proposed MCF Link

The configuration of the proposed system [40], consisting of POSUs and MCFs, is shown in Fig. 6.13. High-capacity signals for an inter-/intra-data center network or PON network are gathered by the FI/FO modules and input into the MCFs. The protection cores for optical signals in each MCF are reserved for redundancy operation. Switching from a signal line to a protection line occurs immediately after a fiber link failure is detected. With this configuration, the proposed system supports large-capacity, high-density and high-reliability transmission simultaneously by using MCFs and POSUs.

6.2.2.2 Components of the Proposed MCF Systems

(1) Protection optical switch units

The fabricated POSU for the MCF link is shown in Fig. 6.14 [40]. It was designed for a link with three seven-core MCFs. The center core carries a control signal; the

Fig. 6.14 Fabricated POSU



other (outer) six cores are used as main and standby signal lines. The unit size is $430 \times 550 \times 132.5$ mm (corresponding to 3U of a 19-inch rack).

The POSU consists of optical switches, a switch-controller board, a field programmable gate array (FPGA), tap photodiode (PD) arrays and optical couplers. A thermo-optic (TO) switch was chosen as the optical switch because it provides high-speed operation as well as low insertion loss operation.

The tap PD monitors optical power of the main signal lines. In the case that unacceptable loss is detected in the main signal line, the FPGA sends a control signal to the switch-controller board, which then automatically switches to the standby signal line for restoration of communication.

(2) *Fan-in/fan-out modules*

We used a seven-core MCF as shown in Fig. 6.15 with a cut-off wavelength below $1.3 \mu\text{m}$ designed for applications in DCs [53]. The mode field diameters (MFDs) of the MCFs were 8.6 to $8.8 \mu\text{m}$ at a wavelength of $1.55 \mu\text{m}$. The average core pitch of the MCFs was $40 \mu\text{m}$.

An FI/FO module based on free-space optics [75] was fabricated to connect MCFs with the SMFs. The free-space optics-based FI/FO module could be applied to a wide range of wavelengths, any number of cores and any core arrangements; i.e., it had design flexibility.

It was necessary to expand the diameters of the light beams from 8.8 to $10.5 \mu\text{m}$ and their spaces from $40 \mu\text{m}$ to more than 0.9 mm to couple each core between the MCF and the SMFs. Figure 6.16 schematically shows the free-space-based FI/FO. Both ends of the MCF and the SMFs were polished flat at an angle. Aspherical lenses

Fig. 6.15 Schematic of cross-section of a seven-core MCF

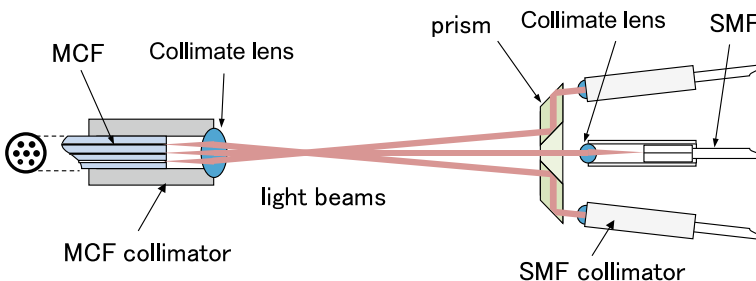
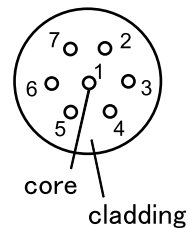


Fig. 6.16 Schematic of free-space-based FI/FO

were located on the ends of the MCF and the SMFs in a confocal arrangement. The diameter of the light beams emitted from the MCF was magnified by 1.2 times at the end of the SMF by these lenses. Six prisms were inserted between six pairs of the lenses to expand the spacing between the light beams. Each facet of the fibers, lenses and prism was coated with an anti-reflective film to obtain transmittance of more than 99% and an optical loss of less than 0.044 dB. The estimated losses between the center core of the MCF and the SMFs were less than 0.26 dB because the light beams passed through six facets of the fibers and lenses in the FI/FO. The estimated losses between the outer cores of the MCFs and SMFs were less than 0.35 dB because the losses of the two facets of the prism in the FI/FO were added to the above.

A SC/PC connector was mounted on the other ends of the MCF, and LC/PC connectors were mounted on the other ends the SMFs. The SC/PC MCF connector is described in Sect. 6.2.2.3–(3) in detail. Figure 6.17 shows a photograph of the fabricated FI/FO. The characteristics of the fabricated FI/FOs are shown in Fig. 6.18. The measured insertion losses of the FI/FOs were less than 0.7 dB (typically 0.3 dB) including the insertion losses of the MCF connectors and return losses that were more than 40 dB.

Fig. 6.17 Photograph of free-space-based FI/FO with fibers

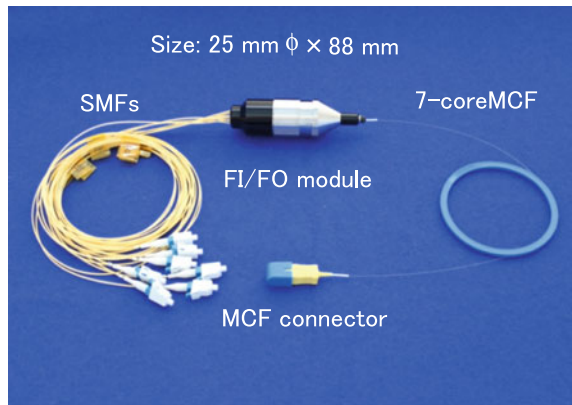
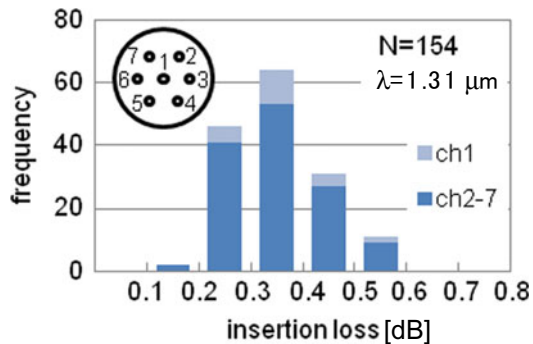


Fig. 6.18 Insertion loss of fabricated FI/FOs measured at wavelength of 1.31 μ m



(3) *MCF connectors*

The fabricated MCF connectors were the widely used SC type [76] with a PC structure [77]. Although the conventional SC type is common, a ferrule freely turns in the connector because of the clearance between the connector housing and the ferrule. When the housing is applied to the connector for MCFs, coupling losses in the outer cores of the MCFs are increased by angular misalignment between the two MCFs.

The coupling loss of the fiber pair can be calculated by using the following Gaussian field approximation [78]:

$$\text{Loss} = -10 \log_{10}(\eta) \tag{6.1}$$

$$\eta = \left(\frac{2\omega_1\omega_2}{\omega_1^2 + \omega_2^2} \right)^2 \exp\left(-\frac{2d^2}{\omega_1^2 + \omega_2^2}\right), \tag{6.2}$$

where d is the core offset and ω_1 and ω_2 are the mode field radii of the pair of cores. Since the range of core pitch errors is 1 μm , the angular misalignment must be reduced to within 0.7 degrees to satisfy a coupling loss of less than 0.5 dB [79] from (6.1) and (6.2). The ferrule is held with a pressurization spring attached to a plug frame in a connector housing to prevent the ferrule from turning [80]. The pressurization spring is a plate spring formed by using sheet metal processing. It has four claws. As we can see from Fig. 6.19, it holds the flange of the ferrule from four directions without slippage in the plug frame. The plug frame is made of plastic molding and has a space into which the pressurization spring is inserted. The ferrule is thus “floating” in the plug frame being held by the four claws of the pressurization spring, and it can only move in the x - and y -directions. A photograph and characteristics of the fabricated connectors are shown in Fig. 6.20 [80]. The measured insertion losses of the connectors are less than 0.5 dB (typically 0.2 dB), and the return losses are more than 40 dB.

Furthermore, we fabricated LC-type MCF connector by using the same technique as used to fabricate SC-type connector (see Fig. 6.21). The LC-type connector is four

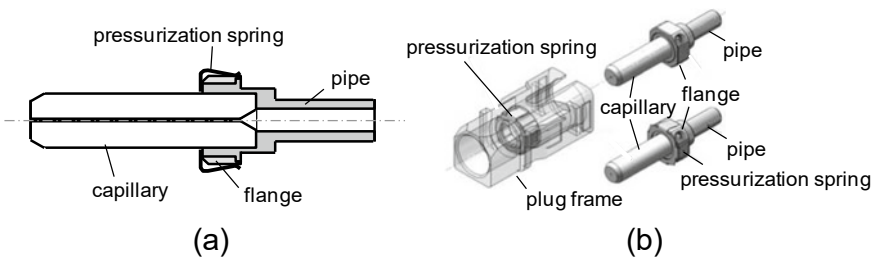


Fig. 6.19 Schematic structure of ferrule fixed in plug frame with pressurization spring: **a** Cross-section of ferrule and **b** Bird's eye view

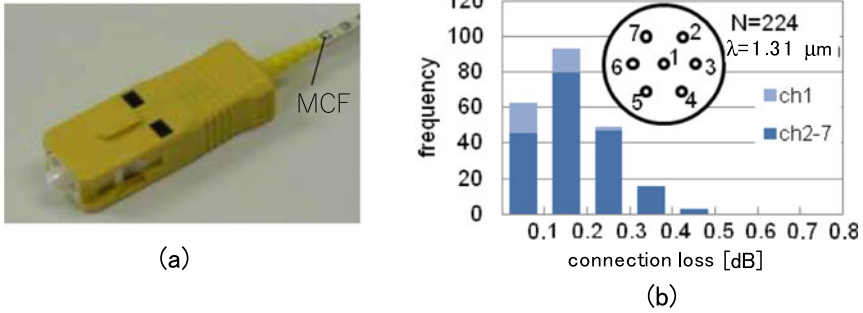
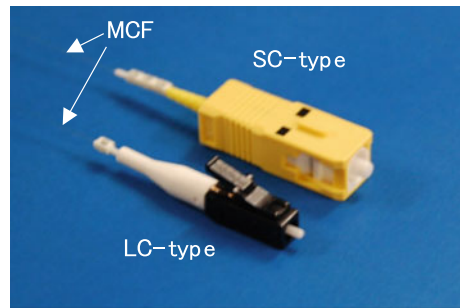


Fig. 6.20 **a** Fabricated SC-type MCF connector **b** Connection loss of the SC-type MCF connectors measured at 1.31 μm wavelength

Fig. 6.21 Photographs of a fabricated LC-type MCF connector together with the SC-type connector for comparison



times smaller than SC type and widely used in data centers (see DC standard TIA-942). Insertion loss, PDL, connection loss after mating cycles are almost equivalent to those of the SC-type connector as shown in Table 6.2.

6.2.2.3 MCF Link Based on Multi-ring Structure

Protecting the paths substituted for working paths needs to be adequately arranged in links between the centralized node as the I/O interface and its branch nodes to construct a robust network with high levels of reliability in access areas such as DCs and FTTH systems. We considered a ring network topology and MCF in the present study, which were able to cope with ultra-large data [81, 82]. The ring network topology provided promise in terms of helping to increase performance, e.g., to ensure highly reliable characteristics while maintaining large-capacity transmission in such networks. We, therefore, constructed a link based on a multi-ring structure where an MCF link [82] was used to connect nodes. Such MCF links can make connections between centralized nodes and their branch nodes through various routes.

Figure 6.22 is a schematic of the proposed ring network topology. One POSU with an optical SW is located at a centralized node, and POSUs with optical SWs are

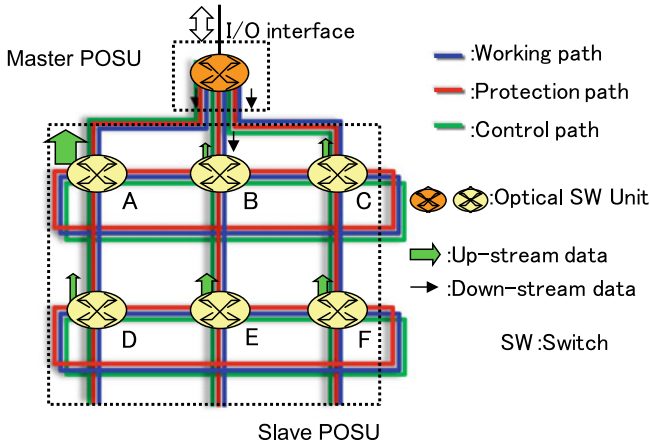


Fig. 6.22 MCF link for highly reliable network

arranged at branch nodes (A, B, C, D, E and F). The link between units is connected by just one MCF constituting a one-ring structure via Nodes A, B and C. An additional unit at Node D can be linked by a cascade connection with the unit at Node A by just one MCF. Similarly, units at Nodes E and F can be linked with units B and C by just one MCF. These links also constitute a one-ring structure by using Nodes D, E and F. The unit at centralized Node Z plays a master role, and the units at its branch nodes of A, B, C, D, E and F play slave roles.

Since this topology can easily be used to set up branch nodes due to cascade connections, it has an advantage in terms of scalability. Moreover, this MCF link based on a multi-ring structure undeniably leads to increased network performance, viz., various kinds of paths (e.g., working, protection and control) can be flexibly laid on the links because of the use of multiple cores in just one MCF. This enables us to secure a protected path substituting for failures in working paths even if network failure occurs. As was previously stated, we could construct a network with strong capacity, scalability, flexibility and reliability characteristics by using an MCF link based on a multi-ring structure.

Furthermore, the MCF link communicates with data between the master unit and the slave units by means of bidirectional transmissions through working/protection paths, as outlined in the upstream/downstream data in Fig. 6.22. The MCF link can assign multiple paths in addition to the working path, thus increasing the transmission capacity from the node when upstream data from a node increases in the ordinary operating mode, as indicated in Fig. 6.22. The units at the nodes can share network information indicating failure alarms/notifications, restoration requests/replies and switch configurations by using the control paths.

However, a control architecture is needed to switch from a working path to a protective path in the event of link or node failure to manage the MCF link based on the multiple ring structure. We proposed a failure recovery scheme to manage the

link by means of monitoring signals (FRS-MS) [83] to cope with multiple failures in not only the working paths, but also the protective paths of the link. Figure 6.23 shows a schematic of the link, which is structured between two nodes with switch (SW) units. The link between units is constructed by assigning paths a, b and c as working paths and paths d, e and f as protective paths (Fig. 6.23a). MCFs are all that are needed because they have multiple cores, and we can freely assign working and protective paths to the cores in the link connected by MCFs when designing a network to fit the specific needs of applications, such as high capacity through the use of *switch database management* (SDM) technology [36] and high reliability through using restoration schemes by using protective paths. Moreover, the MCF connection has advantages in terms of handling and the space it occupies in comparison with connections using various kinds of fibers such as ribbon and bundle fibers.

The POSU in Fig. 6.23 has an optical SW for transferring paths, a controller for controlling other units and itself and multiple signal detectors for detecting path

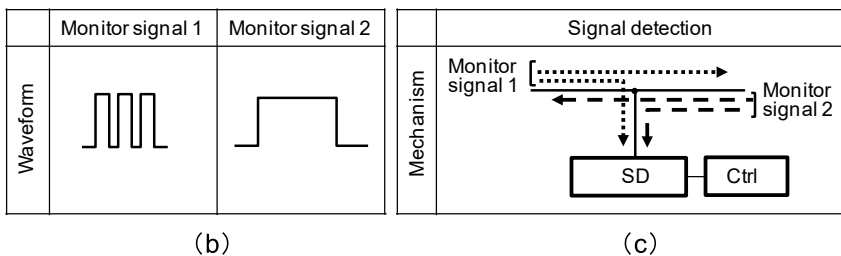
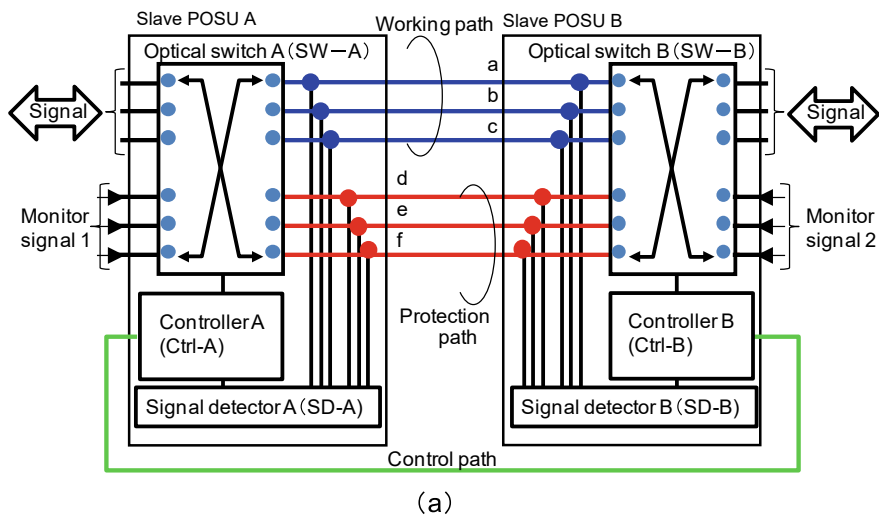


Fig. 6.23 Schematic of failure recovery scheme that sends monitoring signals through protection paths: **a** Switch units consisting of controllers and signal detectors have multiple ports for in/outputting signals and multiple ports for inputting monitoring signals, **b** Waveform of monitoring signals and **c** Mechanism for detecting monitoring signals

failures. The controller (Ctrl-A) in one unit is connected to Ctrl-B in the other by a control path, as seen in Fig. 6.23a. In addition to the input and output ports for the signals, the unit has input ports for the monitoring signals that are needed in FRS-MS. Since monitoring signals such as laser light from the input ports can always be transmitted through protection paths and be observed by the signal detectors (SD-A/SD-B) in this link, we can check the propriety of path usage before switching operations are carried out. In addition, a monitoring signal helps to secure a protective path for the working path because we can use it to find the most available path in the protective paths. FRS-MS can work by doing just one switching procedure due to its control of all-optical POSUs at each node in the MCF link based on the multiple ring structure, which shortens the recovery time.

Moreover, a link based on FRS-MS can distinguish link failure from component failure. For instance, the waveform of Monitoring Signal 1 incoming to POSU A is different from that of Monitoring Signal 2 incoming to POSU B in Fig. 6.23b. The signal detector can, hence, distinguish a monitoring signal from the right from one from the left in Fig. 6.23c. Hence, when SD-A in POSU A detects Monitoring Signal 2 instead of Monitoring Signal 1 and SD-B in POSU B detects Monitoring Signal 2 instead of Monitoring Signal 1, we can determine that there has been a failure in optical switch A (SW-A) as opposed to failure in one of the working paths without failure in optical switch B (SW-B). However, when SD-A in POSU A detects Monitoring Signal 1 instead of Monitoring Signal 2 and SD-B in POSU B detects Monitoring Signal 2 instead of Monitoring Signal 1, we can determine that there has been a failure in one of the working paths as opposed to failure in optical SW-A without failure in SW-B. This function helps to inspect the paths between units, diagnose the optical switches in units and exchange the failure components and fibers, which thereby easily helps to maintain the network. Hence, we could suitably manage the network and consequently increase its reliability by implementing such FRS-MS on FPGA in units at nodes in the MCF link based on the multiple ring structure.

6.2.2.4 Recovery from Failure in an MCF Link

This section describes the experimental setup for testing recovery from a link failure. Next, we will discuss the experimental evaluation in terms of the operation of this MCF link in the event of a link failure.

(1) *Setup for evolution of recovery*

We experimentally investigated fundamental operations with relation to the reliability of the proposed MCF link. Figure 6.24 shows the MCF link based on a one-ring structure, which consists of Unit Z as a master and Units A, B and C as slaves. These latter three units are all located on one ring. Each unit has a 20×20 thermo-optical SW for transferring paths, tap PDs for detecting link failure, lasers with a wavelength of $1.5 \mu\text{m}$ for monitoring the protecting paths, two kinds of field programmable gate arrays (FPGAs) (FPGA-A and FPGA-B) for controlling the

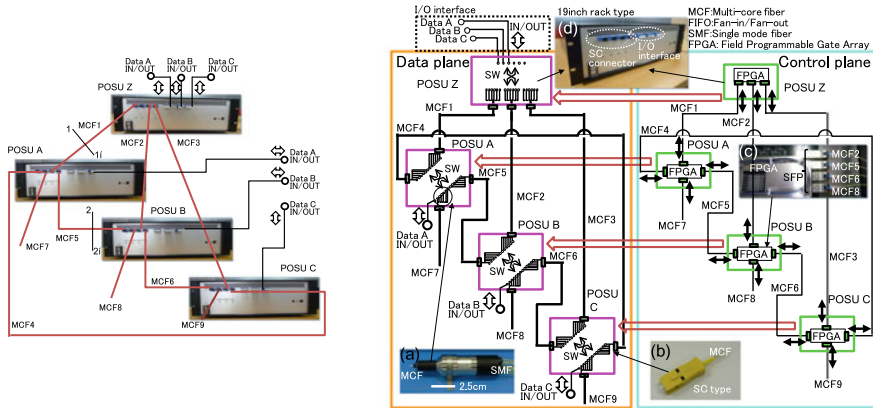


Fig. 6.24 MCF link based on one-ring structure: **a** MCF FI/FO module, **b** MCF connector, **c** FPGA-based control board in unit where outgoing data from control board transmit and receive via optical signals through small form-factor pluggable (SFP) modules and **d** Front panel of unit settled in 19-in. rack. Black arrows indicate bidirectional communication between FPGAs in units, and red-lined arrows indicate control of optical switches by FPGAs in units. Cross-sectional images of 1–1' in MCF1 and of 2–2' in MCF5 are depicted in Table 6.3

MCF link (Fig. 6.24c), four fan-in/fan-out modules for connecting the MCF to each port of an SW (Fig. 6.24a) and four MCF connectors for connecting the MCF to a unit (Fig. 6.24b). The FI/FO modules and MCF connectors are explained in detail in the following Subsections (2) and (3). All components in each unit are accommodated in a 19-inch rack, as shown in Fig. 6.24d. Figure 6.24 also shows that this optical SW allows data incoming to a unit to transfer to two units, although the unit is related to four units arranged around itself. For instance, incoming data to Unit A through MCF1 can exit through MCF5 or MCF7 and are prevented from exiting through MCF4, while the FPGA in the unit can communicate with those in all four units located around itself by means of bidirectional transmission using the controlling path. As an example, the FPGA in Unit A can communicate with all other FPGAs in units that are connected by MCF1, MCF4, MCF7 and MCF5. As a result, all FPGAs around the unit can share network information with one another, even if failure occurs anywhere in the network.

Our MCF link was organized with a data plane for data transmission and with a control plane for FPGA-based management, as seen in Fig. 6.24. Incoming Data A,

Table 6.3 Summary of characteristic of LC- and SC-type MCF connectors

	SC type	LC type
Size of cross-section (mm ²)	9 × 7.5	4 × 5
Insertion loss (dB)	< 0.5	< 0.4
PDL (dB)	< 0.03	< 0.01
Connection loss after ten mating cycles (dB)	< 0.4	< 0.5

B and C to Unit Z (downstream) in the data plane can be output from Units A, B and C by working paths that lead to these units by way of MCFs 1, 2 and 3 after Unit Z in the ordinary operating mode. When we refer to the number of unit passages in a path as the “hop count,” each path, therefore, corresponds to a hop count of two in the ordinary operating mode. Similarly, Incoming Data A, B and C to Units A, B and C (upstream) can be output from Unit Z together by using the same paths downstream. In contrast, FPGA-A detects network failures in the control plane and determines the protecting path as a switching destination from the failure working path on the basis of the switching control architecture mentioned in the previous section. FPGA-B controls the SW in each unit accordance with a command from FPGA-A, as indicated by the red-lined arrows in Fig. 6.24.


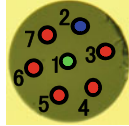





The link between units seen in the data and control planes is connected by just one MCF with seven cores with a length of 100 m. This connection by MCF actually enables us to provide protection and control paths as well as a working path by using just one fiber. Table 6.3 summarizes the assignment of working, protection and control paths for seven cores in the MCFs in the search for designing a network from the viewpoint of reliability. Core 2, Cores 3–7 and Core 1 in MCF1, MCF2 and MCF3 play the roles of working, protection and control paths, respectively, while Cores 2–7 and Core 1 in MCF4, MCF5 and MCF6 play the roles of protection and control paths, respectively. We assigned a control path to Core 1, which was somewhat influenced by crosstalk from the other cores (inset: Table 6.3) [84, 85], because a signal in the control path could be enhanced in terms of the signal-to-noise ratio. Thus, this assignment in the MCF link effectively contributed to securing a protection path when failure occurred in the network.

We used the laser lights of the wavelengths in the C-band in these experiments as the incoming data to the I/O interface in Unit Z. The laser lights of the outgoing data from Units A, B and C were measured with an oscilloscope (Agilent: MSO6104A) through an optical/electronic (O/E) converter and with an optical spectrum analyzer (Anritsu: MS6710A). In addition, all outgoing electronic signals (P1, P4 and P8) from the control board in each unit indicated the detection of network failure by FPGAs, the operation of SW driven by FPGAs and the detection of data signals by FPGA, respectively, and were observed with the same oscilloscope. We could accurately estimate the recovery time by using P1, P4 and P8 from that in Unit Z and trace the protecting path as the switching destination with P4 in all units (Table 6.4).

(2) Automatic switching for recovery from fiber failure

Figure 6.25 shows the signals for the outgoing data from Units A, B and C and that of the outgoing electronic signals from the control board in all units when failure occurred in MCF1 between Unit Z and Unit A in Fig. 6.24. Automatic impairment-aware optical-path switching was done in the MCF link based on a one-ring structure in the event of MCF1 failure. As a result, only the signal of Data A with laser light that had a 1.54 μm wavelength, which was transmitted to Unit A from Unit Z, was intercepted and subsequently recovered, as shown in Figs. 6.25a, c, d. We estimated the recovery time to be $\Delta T = 7.4$ ms by using P1, P4 and P8 from the control board in Unit Z, as shown in Fig. 6.25b. This time was sufficiently less than that required by the

Table 6.4 Assignment of working/protection/control paths for seven cores in MCFs

Path name	MCF1/MCF2/MCF3		MCF4/MCF5/MCF6	
	Arrangement	Cross-section	Arrangement	Cross-section
Working	Core2 		–	
Protecting	Core3,4,5,6,7 		Core2,3,4,5,6,7 	
Control	Core1 		Core1 	

Telecommunication Standardization Sector of the International Telecommunication Union (ITU-T) [86]. This is because the protection path substituted for the failure working path was immediately secured when failure occurred in MCF1.

Figure 6.25 presents signals of Data A and B with laser light that had a wavelength of 1.55 μm, which were transmitted to Unit B from Unit Z, and Data C with a wavelength of 1.56 μm, which were transmitted to Unit C from Unit Z, in the ordinary operating mode (c) and after switching operation (d), when failure occurred in MCF1. The working path in the ordinary operating mode for Data A, which led to Unit A through the working path in MCF1 after unit Z, corresponds to a hop count of two. Data A in the MCF link is recovered with an optical loss of $\Delta L = 7.4$ dB after switching operation, as shown in Figs. 6.25 (c) and (d), which is equivalent to a transmission loss for one unit. We estimated one unit to have an 8.6 dB transmission loss as the sum of the component insertion loss of 0.6 dB at two MCF FI/FO modules, 0.4 dB at two MCF connectors, 4.0 dB at optical SW, 1.2 dB at six fiber junctions and 2.4 dB at four points inserted by tap PD. This means that, a loss for a unit increases in the protection path for Data A. The path, hence, must have a hop count of three, viz., the protection path leads to Unit A through a protection path in MCF4 by way of Unit C through a protection path in MCF3 after Unit Z. Transmission through this path after failure can be explicitly confirmed by the dependence on time with the pulse shape of outgoing electronic signals P4 from Units B, C and Z with no change in dependence on time from that of Unit A, as shown in Fig. 6.25 (e). Therefore, we can draw working paths in the ordinary operating mode and working/protection paths after switching operations in Figs. 6.26a, b. An incoming signal to a unit is only allowed to exit using permitted paths through an optical SW in the MCF link, as shown in Fig. 6.24. However, despite this restriction, we can select a path with the lowest loss from several paths from Units Z to A, except for a path in the ordinary operating mode, due to the switching control architecture proposed in this paper. As a result, the MCF link enables us to suppress any increase in the hop count causing low-loss transmission after switching operation.

Figures 6.25a, c, d indicate that the MCF link based on a one-ring structure kept the outgoing signals of Data B and C transmitting, regardless of failure in MCF1. This meant that, the process of switching to a protection path from a working path for Data A did not interrupt the transmission of Data B or C. This is because MCF3 had

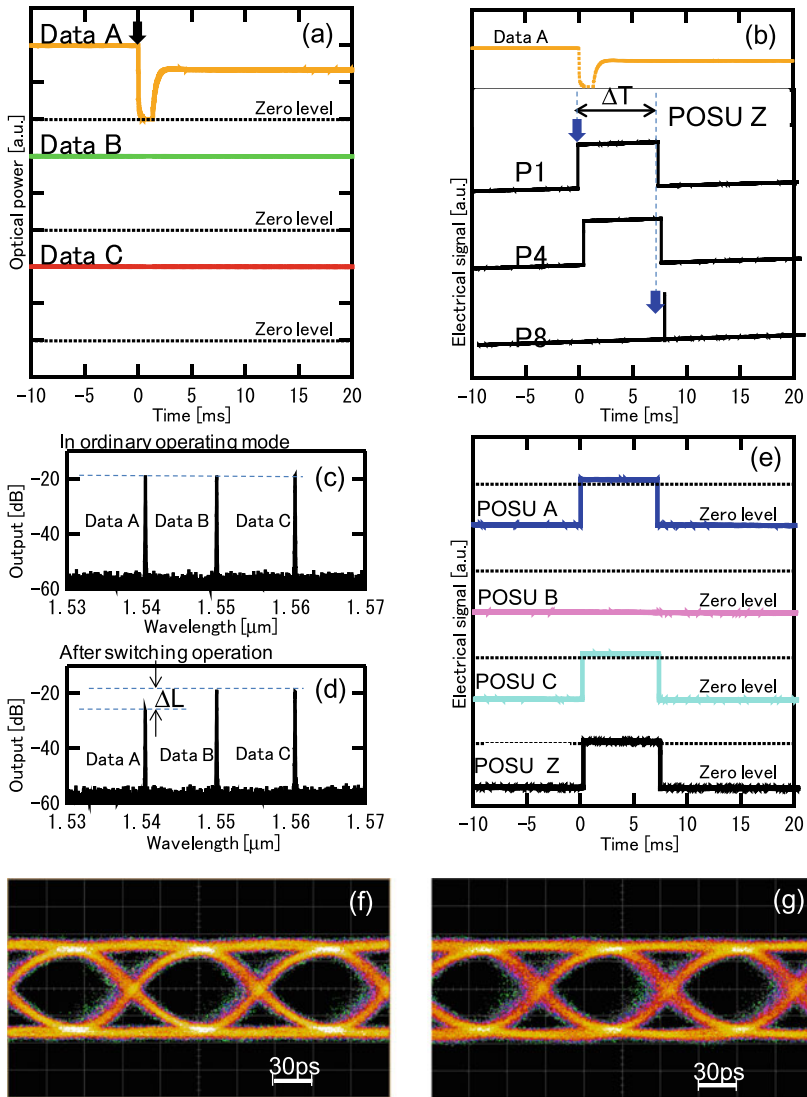


Fig. 6.25 Signals for data transmission in MCF link and that of outgoing electronic signals from control board in units when failure occurred in MCF1 in Fig. 6.24: **a** Dependence of outgoing signals of Data A, B and C on time from Units A, B and C, **b** Dependence of outgoing electronic signals P1, P4 and P8 on time from that in Unit Z, **c** Outgoing signals of Data A, B and C from Units A, B and C in ordinary operating mode, **d** Outgoing signals of Data A, B and C from Units A, B and C after switching operation for recovery and **e** Dependence of outgoing electronic signals P4 from FPGAs on time in Units A, B, C and Z. Electrical eye diagrams of outgoing data from Unit C, **f** In ordinary operating mode and **g** After switching operation for recovery

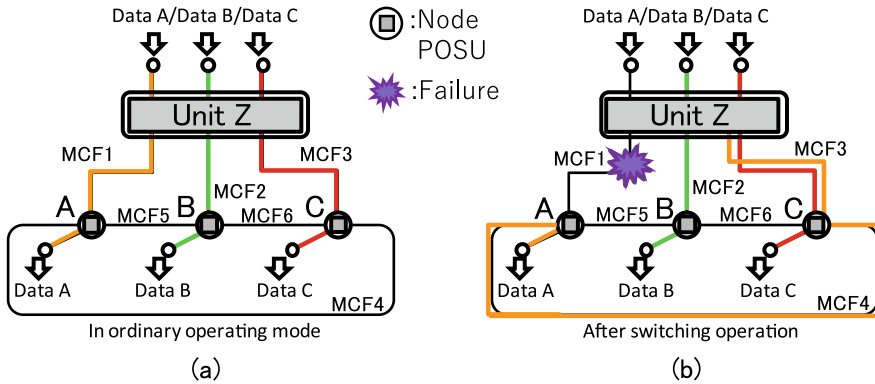


Fig. 6.26 Paths for data transmission in MCF link when failure occurred in MCF1 in Fig. 6.24: **a** Working paths in ordinary operating mode and **b** Working and protection paths after switching operation for recovery, when failure occurred in MCF1

both a working path for accessing Unit C and a protection path for accessing Unit A, as listed in Table 6.3. Figure 6.25e also shows that the optical switch modules in Units A, C and Z operate simultaneously in laying the protection path. We can secure a protection path to substitute for a failed working path for Data A in just one switching process. The relatively short recovery time, as was previously mentioned, can be attributed to this switching process.

We next examined the high bit-rate performance of data transmission between units in the MCF link. Direct digital modulation transfer between units was carried out using a conventional 10 Gbit/s form-factor pluggable (XFP) module modulated by a non-return-to-zero (NRZ) data format with a $2^{31}-1$ pseudorandom binary sequence (PRBS) at the wavelength of $1.55 \mu\text{m}$ to evaluate data transmission. Figure 6.25 has the measured electrical eye diagrams of outgoing data from Unit A for incoming data to Unit Z. Clear 10-Gb/s eye openings were obtained in ordinary operating mode and after switching operation (see Figs. 6.25f, g). Thus, this indicates that the MCF link could effectively continue data transmission between units even in the event of link failure due to the sophisticated recovery scheme of FRS-MS by using FPGA-based switching units.

Moreover, such a principle of operation in an MCF link based on a one-ring structure can equivalently be applied to that based on a multi-ring structure. Thus, automatic impairment-aware optical-path switching works in the event of multi-failures in the MCF link based on a multi-ring structure.

Conclusions

We presented a novel MCF link based on a multi-ring structure with FPGA-based optical switching units. A switching algorithm implemented in these units was also established in accordance with processes able to cope with link failures in a network, thereby managing this MCF link suitably. Moreover, this link had a connector with a typical connection loss of 0.2 dB, and the FI/FO module had a typical connection

loss of 0.3 dB to connect units with the MCF link. We experimentally demonstrated automatic impairment-aware optical-path switching with FPGA-based control in units to verify the fundamental operation of the proposed link when failure occurred in the MCF link based on a one-ring structure. We succeeded in path recovery by switching operation within a relatively short time of 7.4 ms, which was sufficiently less than that required by the ITU-T (i.e., < 50 ms). The selection of a protecting path to substitute for a failure working path was also optimized as the minimum passage of units for low-loss transmission. These results indicate that our proposed link has the potential for network design with a highly reliable network topology in access areas such as those for DCs and FTTH systems.

Acknowledgements We appreciate Dr. T. Kamiya and Prof. T. Morioka for their support in researching short-reach MCF applications. This work was also partly supported by “The research and development project for the ultra-high speed and green photonic networks” of the Ministry of Internal Affairs and Communications, Japan.

References

1. R. Ryf, S. Randel, A.H. Gnauck, C. Bolle, A. Sierra, S. Mumtaz, M. Esmaelpour, E.C. Burrows, R.-J. Essiambre, P.J. Winzer, D.W. Peckham, A.H. McCurdy, R. Lingle Jr., Mode-division multiplexing over 96 km of few-mode fiber using coherent 6×6 MIMO processing. *J. Lightwave Technol.* **30**(4), 521–531 (2012)
2. H. Takara, A. Sano, T. Kobayashi, H. Kubota, H. Kawakami, A. Matsuura, Y. Miyamoto, Y. Abe, H. Ono, K. Shikama, Y. Goto, K. Tsujikawa, Y. Sasaki, I. Ishida, K. Takenaga, S. Matsuo, K. Saitoh, M. Koshihara, T. Morioka, 1.01-Pb/s (12 SDM/222 WDM/456 Gb/s) crosstalk-managed transmission with 91.4-b/s/Hz aggregate spectral efficiency, in *38th European Conference and Exhibition on Optical Communication (ECOC), paper Th.3.C.1* (2012)
3. T. Mizuno, T. Kobayashi, H. Takara, A. Sano, H. Kawakami, T. Nakagawa, Y. Miyamoto, Y. Abe, T. Goh, M. Oguma, T. Sakamoto, Y. Sasaki, I. Ishida, K. Takenaga, S. Matsuo, K. Saitoh, T. Morioka, 12-core \times 3-mode dense space division multiplexed transmission over 40 km employing multi-carrier signals with parallel MIMO equalization, in *Optical Fiber Communication Conference and Exposition (OFC/NFOEC), paper Th5B.2* (2014)
4. P.J. Winzer, Making spatial multiplexing a reality: the future of high-capacity optical networks. *Nat. Photon.* **8**(5), 345–348 (2014)
5. S.L. Woodward, M.D. Feuer, P. Palarchala, ROADM-node architectures for reconfigurable photonic networks, in *Optical Fiber Telecommunications VIB*, eds. I.P. Kaminow, T. Li, A. Willner (Academic Press, 2013)
6. D.M. Marom, D.T. Neilson, D.S. Greywall, C.-S. Pai, N.R. Basavanahally, V.A. Aksyuk, D.O. López, F. Pardo, M.E. Simon, Y. Low, P. Kolodner, C.A. Bolle, Wavelength-selective $1 \times K$ switches using free-space optics and MEMS micromirrors: theory, design, and implementation. *J. Lightwave Technol.* **23**(4), 1620–1630 (2005)
7. G. Baxter, S. Frisken, D. Abakoumov, H. Zhou, I. Clarke, A. Bartos, S. Poole, Highly programmable wavelength selective switch based on liquid crystal on silicon switching elements, in *Optical Fiber Communication/National Fiber Optic Engineers Conference (OFC/NFOEC), paper OTuF2* (2006)
8. International Telecommunication Union, Spectral Grids for WDM Applications: DWDM Frequency Grid. ITU-T Rec. G.694.1 (2012)

9. M.D. Feuer, L.E. Nelson, K. Abedin, X. Zhou, T.F. Taunay, J.F. Fini, B. Zhu, R. Isaac, R. Harel, G. Cohen, D.M. Marom, ROADM system for space division multiplexing with spatial superchannels, in *Optical Fiber Communication/National Fiber Optic Engineers Conference (OFC/NFOEC)*, paper PDP5B.8 (2013)
10. L.E. Nelson, M.D. Feuer, K. Abedin, X. Zhou, T.F. Taunay, J.M. Fini, B. Zhu, R. Isaac, R. Harel, G. Cohen, D.M. Marom, Spatial superchannel routing in a two-span ROADM system for space division multiplexing. *J. Lightwave Technol.* **32**(4), 783–789 (2014)
11. R. Ryf, N.K. Fontaine, J. Dunayevsky, D. Sinefeld, M. Blau, M. Montoliu, S. Randel, C. Liu, B. Ercan, M. Esmaelpour, S. Chandrasekhar, A.H. Gnauck, S.G. Leon-Saval, J. Bland-Hawthorn, J.R. Salazar-Gil, Y. Sun, L. Gruner-Nielsen, R. Lingle, D.M. Marom, Wavelength-selective switch for few-mode fiber transmission, in *European Conference and Exposition on Optical Communications (ECOC)*, paper PD1C4 (2013)
12. D. Noordegraaf, P.M.W. Skovgaard, M.D. Nielsen, J. Bland-Hawthorn, Efficient multi-mode to singlemode coupling in a photonic lantern. *Opt. Express* **17**(3), 1988–1994 (2009)
13. S.G. Leon-Saval, A. Argyros, J. Bland-Hawthorn, Photonic lanterns: a study of light propagation in multimode to single-mode converters. *Opt. Express* **18**(8), 8430–8439 (2010)
14. J. Carpenter, S.G. Leon-Saval, J.R. Salazar-Gil, J. Bland-Hawthorn, G. Baxter, L. Stewart, S. Frisken, M.A.F. Roelens, B.J. Eggleton, J. Schröder, 1×11 few-mode fiber wavelength selective switch using photonic lanterns. *Opt. Express* **22**(3), 2216–2221 (2014)
15. N.K. Fontaine, T. Haramaty, R. Ryf, H. Chen, L. Miron, L. Pascar, M. Blau, B. Frenkel, L. Wang, Y. Messaddeq, S. LaRochelle, R.J. Essiambre, Y. Jung, Q. Kang, J.K. Sahu, S.U. Alam, D.J. Richardson, D.M. Marom, Heterogeneous space-division multiplexing and joint wavelength switching demonstration, in *Optical Fiber Communication Conference and Exposition (OFC/NFOEC)*, paper Th5C.5 (2015)
16. N.K. Fontaine, R. Ryf, D.T. Neilson, Wavelength selective crossconnects, in *Opto Electronics and Communications Conference (OECC)*, 2013, paper ThT1.4 (2015)
17. Open Networking Foundation, Software-Defined Networking: The New Norm for Networks. ONF White Paper (2012)
18. X. Cao, V. Anand, C. Qiao, Multi-layer versus single-layer optical cross-connect architectures for waveband switching. *IEEE INFOCOM* **2004**, 1830–1840 (2004)
19. N. Amaya, G.S. Zervas, D. Simeonidou, Architecture on demand for transparent optical networks, in *International Conference of Transparent Networks (ICTON)*, paper Th.A1.5 (2011)
20. M. Garrich, N. Amaya, G.S. Zervas, P. Giaccone, D. Simeonidou, Power consumption analysis of architecture on demand, in *European Conference and Exhibition on Optical Communication (ECOC)*, paper P5.06 (2012)
21. N. Amaya, M. Irfan, G. Zervas, R. Nejabati, D. Simeonidou, J. Sakaguchi, W. Klaus, B.J. Puttnam, T. Miyazawa, Y. Awaji, N. Wada, I. Henning, Fully-elastic multi-granular network with space/frequency/time switching using multi-core fibres and programmable optical nodes. *Opt. Express* **21**(7), 8865–8872 (2013)
22. N. Amaya, S. Yan, M. Channegowda, B.R. Rofoee, Y. Shu, M. Rashidi, Y. Ou, E. Hugues-Salas, G. Zervas, R. Nejabati, D. Simeonidou, B.J. Puttnam, W. Klaus, J. Sakaguchi, T. Miyazawa, Y. Awaji, H. Harai, N. Wada, Software defined networking (SDN) over space division multiplexing (SDM) optical networks: features, benefits and experimental demonstration. *Opt. Express* **22**(3), 3638–3647 (2014)
23. N. McKeown, T. Anderson, H. Balakrishnan, G. Parulkar, L. Peterson, J. Rexford, S. Schenker, J. Turner, OpenFlow: enabling innovation in campus networks. *ACM SIGCOMM Comp. Comm. Rev.* **38**(2), 69–74 (2008)
24. S. Fujii, Y. Hirota, T. Watanabe, H. Tode, Dynamic spectrum and core allocation with spectrum region reducing costs of building modules in AoD nodes. *Telecommun. Netw. Strategy Plann. Symp. (Netw.)* **2014**, 1–6 (2014)
25. S. Fujii, Y. Hirota, H. Tode, K. Murakami, On-Demand spectrum and core allocation for reducing crosstalk in multicore fibers in elastic optical networks. *J. Opt. Commun. Netw.* **6**(12), 1059–1071 (2014)

26. E. Ciaramella, Wavelength conversion and all-optical regeneration: achievements and open issues. *J. Lightwave Technol.* **30**(4), 572–582 (2012)
27. R.S. Luís, B.J. Puttnam, J.-M.D. Mendinueta, W. Klaus, Y. Awaji, N. Wada, Comparing inter-core skew fluctuations in multi-core and single-core fibers, in *Conference on Lasers and Electro-Optics (CLEO), paper SM2L.5* (2015)
28. M.D. Feuer, L.E. Nelson, X. Zhou, S.L. Woodward, R. Isaac, B. Zhu, T.F. Taunay, M. Fishteyn, J.M. Fini, M.F. Yan, Joint digital signal processing receivers for spatial superchannels. *Phot. Techn. Lett.* **24**(21), 1957–1960 (2012)
29. T. Ito, E.L.T. de Gabory, M. Arikawa, Y. Hashimoto, K. Fukuchi, Reduction of Influence of inter-core cross-talk in MCF with bidirectional assignment between neighboring cores, in *Optical Fiber Communication Conference and Exposition (OFC/NFOEC), paper OTh3K.2* (2013)
30. F. Ye, T. Morioka, Interleaved core assignment for bidirectional transmission in multi-core fibers, in *European Conference and Exhibition on Optical Communication (ECOC), paper We.2.D.5* (2013)
31. S.K. Korotky, Semi-empirical description and projections of internet traffic trends using a hyperbolic compound annual growth rate. *Bell Labs Techn. J.* **18**(3), 5–21 (2013)
32. Network Disaster Recovery. *IEEE Commun. Mag.* **49**(1) (2011)
33. S. Secci, S. Murugesan, Cloud networks: enhancing performance and resiliency. *IEEE Comput.* 82–85 (2014)
34. R.E. Krock, Lack of emergency recovery planning is a disaster waiting to happen. *IEEE Commun. Mag.* 48–51 (2011)
35. K.T. Morrison, Rapidly recovering from the catastrophic loss of a major telecommunications office. *IEEE Commun. Mag.* 28–35 (2011)
36. J. Sakaguchi, B.J. Puttnam, W. Klaus, Y. Awaji, N. Wada, A. Kanno, T. Kawanishi, K. Imamura, H. Inaba, K. Mukasa, R. Sugizaki, T. Kobayashi, M. Watanabe, 305 Tb/s space division multiplexed transmission using homogeneous 19-core fiber. *IEEE J. Lightwave Technol.* **31**(4), 554–562 (2013)
37. H. Takara, H. Takara, A. Sano, T. Kobayashi, H. Kubota, H. Kawakami, A. Matsuura, Y. Miyamoto, Y. Abe, H. Ono, K. Shikama, Y. Goto, K. Tsujikawa, Y. Sasaki, I. Ishida, K. Take-naga, S. Matsuo, K. Saitoh, M. Koshiha, T. Morioka, 1.01-Pb/s (12 SDM/222 WDM/456 Gb/s) crosstalk-managed transmission with 91.4-b/s/Hz aggregate spectral efficiency, in *Proceedings of European Conference of Optical Communication (ECOC), PDP Th.3.C.1*, Amsterdam (2012)
38. B. Zhu, T.F. Taunay, M.F. Yan, J.M. Fini, M. Fishteyn, E.M. Monberg, F.V. Dimarcello, Seven-core multicore fiber transmissions for passive optical network. *Opt. Express* **18**(11), 11117–11122 (2010)
39. K. Hiruma, T. Sugawara, K. Tanaka, E. Nomoto, Y. Lee, Proposal of high-capacity and high-reliability optical switch equipment with multi-core fibers, in *Proceedings of the 18th Opto Electronics and Communications Conference (OECC), paper ThT1-2*, Kyoto, July (2013)
40. Y. Lee, K. Tanaka, K. Hiruma, E. Nomoto, T. Sugawara, H. Arimoto, Experimental demonstration of a highly reliable multicore-fiber-based optical network. *IEEE Photon Technol. Lett.* **26**(6), 538–540 (2014)
41. Y. Lee, K. Tanaka, K. Hiruma, E. Nomoto, T. Sugawara, H. Arimoto, Multi-core fiber technology for optical-access and short-range links, in *Proceedings of the 12th International Conference on Optical Internet (COIN), TB2-4* (2014)
42. C.J.S. DeCusatis, A. Carranza, C.M. DeCusatis, Communication within clouds: open standards and proprietary protocols for data center networking. *IEEE Commun. Mag.* 26–33 (2012)
43. T. Mitsui, T. Sakamoto, K. Hara, N. Yoshimoto, “flexible and scalable PON protection architecture using N:M redundancy toward next generation access network, in *Proceedings of The 17th Asia-Pacific Conference on Communications (APCC)*, pp. 224–229, October (2011)
44. T. Costello, *Business Continuity: Beyond Disaster Recovery*, pp. 62–64, IT Pro September/October (2012)

45. S. Senda, K. Nguyen, S. Yamada, Requirements for resilient information and communication technology, in *Proceedings of 2013 Seventh International Conference on Complex, Intelligent, and Software Intensive Systems (CISIS)*, Taichung, Taiwan, pp. 418–423 (2013)
46. C. DeCusatis, Optical interconnect networks for data communications. *IEEE J. Lightwave Technol.* **32**(4), 544–552 (2014)
47. S. Azodolmolky, P. Wieder, R. Yahyapour, Cloud computing networking: challenges and opportunities for innovations. *IEEE Commun. Mag.* 54–62 (2013)
48. A. Vahdat, The impact of mega-scale data centers on internet architecture, in *Proceedings of Optical Fiber Communication Conference (OFC), MD3.1*, San Diego, CA, pp. 131–132 (2009)
49. A. Vahdat, M. Al-Fares, N. Farrington, R.N. Mysore, G. Porter, S. Radhakrishnan, Scale-out networking in the data center. *IEEE Micro*, 29–41 (2010)
50. B. Welch, G. Nicholl, K. Conroy, J. Maki, D. Lewis, 400G-PSM4: A proposal for the 500 m objective using 100 Gb/s per lane signaling, in Contribution to IEEE 802.3bs 400 Gb/s Ethernet Task Force, Interim Meeting, Pittsburgh, PA, USA, May (2015)
51. R. Hirai, H. Toyoda, N. Kikuchi, Feasibility study of 100 G/lambda Nyquist-PAM4 with commercially available 1.3 μm /1.5 μm EML, in Contribution to IEEE 802.3bs 400 Gb/s Ethernet Task Force, Plenary Meeting, Ottawa, Ontario, CANADA, September (2014)
52. IEEE P802.3bs MMF Ad Hoc, 400 Gb/s 100 m MMF reach objective draft baseline proposal, in Contribution to IEEE 802.3bs 400 Gb/s Ethernet Task Force, Plenary Meeting, San Antonio, TX, USA, November (2014)
53. H. Liu, C. F. Lam, C. Johnson, Scaling optical interconnects in datacenter networks opportunities and challenges for WDM, in *Proceedings of 18th IEEE Symposium on High Performance Interconnects*, pp. 113–116 (2010)
54. B. Zhu, T.F. Taunay, M.F. Yan, M. Fishteyn, G. Oulundsen, D. Vaidya, 70-Gb/s multicore multimode fiber transmissions for optical data links. *IEEE Photon. Technol. Lett.* **22**(22), 1647–1649 (2010)
55. B.G. Lee, D.M. Kuchta, F.E. Doany, C.L. Schow, P. Pepeljugin, C. Baks, T.F. Taunay, B. Zhu, M.F. Yan, G.E. Oulundsen, D.S. Vaidya, W. Luo, N. Li, End-to-end multicore multimode fiber optic link operating up to 120 Gb/s. *IEEE J. Lightwave Technol.* **30**(6), 886–892 (2012)
56. Y. Sun, R. Shubochkin, B. Zhu, Space division multiplexing in access networks, in *Proceedings of SPIE*, 9387, San Francisco, USA (2015)
57. Y. Geng, S. Li, M.-J. Li, C.G. Sutton, R.L. McCollum, R.L. McClure, A.V. Koklyushkin, K.I. Matthews, J.P. Luther, D.L. Butler, High-speed, bi-directional dual-core fiber transmission system for high-density, short-reach optical interconnects, in *Proceedings of SPIE*, 9390, San Francisco, USA (2015)
58. B. Rosinski, J.D. Chi, P. Grosso, J.L. Bihan, Multichannel transmission of a multicore fiber coupled with VCSEL. *IEEE J. Lightwave Technol.* **17**(5), 807–810 (1999)
59. M-J Li, B. Hoover, V.N. Nazarov, D.L. Butle, Multicore fiber for optical interconnect applications, in *Proceedings 17th Opto-Electronics and Communications Conference, paper 5E4-2* (OECC 2012), Busan, Korea, July 2012
60. T. Hayashi, T. Nakanishi, K. Hirashima, O. Shimakawa, F. Sato, K. Koyama, A. Furuya, Y. Murakami, T. Sasaki, 125- μm -cladding 8-core multi-core fiber realizing ultra-high-density cable suitable for O-band short-reach optical interconnects, in *Proceedings of Optical Fiber Communication Conference (OFC)*, Los Angeles, CA, March, 2015, post-deadline paper Th5C.6 (2015)
61. T. Kuri, H. Harai, N. Wada, T. Kawanishi, M. Hosokawa, Adaptable access system: pursuit of ideal future access system architecture. *IEEE Netw. Mag.* **26**(2), 42–48 (2012)
62. F.J. Effenberger, Space division multiplexing in access networks, in *Proceedings of SPIE*, 9387, San Francisco, USA (2015)
63. B. Li, Z. Feng, M. Tang, Z. Xu, S. Fu, Q. Wu, L. Deng, W. Tong, S. Liu, P. Shum, Experimental demonstration of large capacity WSDM optical access network with multicore fibers and advanced modulation formats. *Opt. Express* **23**(9), 10977–11006 (2015)

64. T. Hu, J. Li, P. Zhu, Q. Mo, Y. Ke, C. Du, Z. Liu, Y. He, Z. Li, Z. Chen, Experimental demonstration of passive optical network based on mode-division-multiplexing, in *Proceedings of Optical Fiber Communication Conference (OFC), paper Th2A.63*, Los Angeles, CA, March, 2015
65. K. Nakanishi, S. Yoshida, S. Aoyagi, A low loss multiplexing scheme for PDS system, in *IEICE General Conference, B-10-112*, p. 621 (1997) (in Japanese)
66. N. Cheng, Z. Liao, F.J. Effenberger, Large splitting and long reach passive optical networks with mode coupling receivers, in *Proceedings of 36th European Conference on Optical Communication (ECOC 2010), paper Tu.5.B.3*, Torino, Italy, September, 2010 (2015)
67. M. Fujiwara, K. Suzuki, N. Yoshimoto, M. Oguma, S. Soma, Increasing splitting ratio of 10 Gb/s-class PONs by using FW-DMF, in *Optical Fiber Communication Conference (OFC), paper Tu.2.C.5*, San Francisco, CA, March, 2014 (2014)
68. C. Xia, N. Chand, A.M. Velázquez-Benítez, Z. Yang, X. Liu, J.E. Antonio-Lopez, H. Wen, B. Zhu, N. Zhao, F.J. Effenberger, R. Amezcua-Correa, G. Li, Time-division-multiplexed few-mode passive optical network. *Opt. Express* **23**(2), 1151–1158 (2015)
69. Y. Fang, J. Yu, N. Chi, J. Zhang, J. Xiao, A novel PON architecture based on OAM multiplexing for efficient bandwidth utilization. *IEEE Photon. J.* **7**(1), 1–6 (2015)
70. C. Raffaelli, R. Veisllari, Scheduling and performance of hybrid traffic in a data center optical core switch, in *Proceedings of 16th International Conference on Transparent Optical Networks (ICTON), paper B1.1*, Graz, Austria, July, 2014
71. S. Zhong, Z. Zhu, Optical virtual switching (OvS): a distributed optical switching fabric for intra-data center networking, in *Proceedings of 23rd Wireless and Optical Communication Conference (WOCC), paper O2.3*, Newark, NJ, U.S.A., May 2014
72. M. Fiorani, M. Casoni, S. Aleksic, Large data center interconnects employing hybrid optical switching, in *Proceedings of 18th European Conference on Network and Optical Communications (NOC) and 8th Conference on Optical Cabling and Infrastructure (OC&i)*, July, 2013, pp. 61–68
73. S. Yan, E. Hugues-Salas, V.J.F. Ranaño, Y. Shu, G.M. Saridis, B.R. Rofoee, Y. Yan, A. Peters, S. Jain, T. May-Smith, P. Petropoulos, D.J. Richardson, G. Zervas, D. Simeonidou, Archon: a function programmable optical interconnect architecture for transparent intra and inter data center SDM/TDM/WDM networking. *IEEE J. Lightwave Technol.* **33**(8), 1586–1595 (2015)
74. V.J.F. Ranaño, S. Jain, T.C. May-Smith, E. Hugues-Salas, S. Yan, G. Zervas, D. Simeonidou, P. Petropoulos, D.J. Richardson, Demonstration of space-to-wavelength conversion in SDM networks. *IEEE Photon. Technol. Lett.* **27**(8), 828–83 (2015)
75. Y. Tottori, T. Kobayashi, M. Watanabe, Low Loss optical connection module for seven-core multicore fiber and seven single-mode fibers. *IEEE Photon. Technol. Lett.* **24**(21), 1926–1928 (2012)
76. E. Sugita, R. Nagase, K. Kanayama, T. Shintaku, SC-type single-mode optical fiber connectors. *IEEE J. Lightwave Technol.* **7**, 1689–1696 (1989)
77. K. Shikama, Y. Abe, S. Yanagi, T. Takahashi, Physical-contact conditions for multicore fiber optical connectors, in *Proceedings of Optical Fiber Communication Conference (OFC), paper OM3I.1*, Anaheim, CA, March (2013)
78. D. Marcuse, Loss analysis of single-mode fiber splices. *Bell Syst. Techn. J.* **56**, 703–718 (1977)
79. International Standard, IEC 60874-14-5 First edition 1997–06. Connectors for optical fibres and cables. Part 14-5: Detail specification for fibre optical connector type SC-PC untuned terminated to single-mode fibre type B1.
80. E. Nomoto, K. Hiruma, T. Sugawara, K. Tanaka, and “connectors for optical fibres and cables”, SC-type multi-core optical-fiber connectors using a pressurization spring. *Opt. Rev.* (2015). <https://doi.org/10.1007/s10043-015-0.127-0>
81. N. Farrington, A. Andreyev, Facebook’s Data Center Network Architecture, in *Proceedings of IEEE Optical Interconnects Conference*, Santa Fe, New Mexico, May (2013)
82. B. Zhu, T.F. Taunay, M.F. Yan, M. Fishteyn, G. Oulundsen, D. Vaidya, 70-Gb/s multicore multimode fiber transmissions for optical data links. *IEEE J. Lightwave Technol.* **22**(22), 1647–1649 (2010)

83. K. Tanaka, Y. Lee, E. Nomoto, T. Sugawara, H. Arimoto, Experimental evaluation of recovery from multiple failures in multi-core fiber links using FPGA-based optical switch units. *IEEE J. Lightwave Technol.* **33**(1), 201–211 (2015)
84. J. Sakaguchi, Y. Awaji, N. Wada, Fundamental study on new characterization method for crosstalk property of multi-core fibers using long wavelength probe signals, in *Proceedings of Optical Fiber Communication Conference (OFC), OW1K.1*, Anaheim, CA, March (2013)
85. T. Hayashi, T. Nakanishi, T. Sasaki, K. Saitoh, M. Koshiba, Dependence of crosstalk increase due to tight bend on core layout of multi-core fiber, in *Proceedings of Optical Fiber Communication Conference (OFC), W4D.4*, San Francisco, CA, March (2014)
86. Telecommunication Standardization Sector of International Telecommunication Union (ITU-T). Transmission System and Media. Digital System and Networks G.841